Copyright

by

Julie Alaniz

2017

The Thesis Committee for Julie Alaniz
Certifies that this is the approved version of the following thesis:

New Developments in Texaphyrin Chemistry

Approved By

Supervising Committee:

Supervisor:

_____

Jonathan L. Sessler

_____

Reader: Emily Que

New Developments in Texaphyrin Chemistry

by

Julie Alaniz

Thesis

Presented to the Faculty of the Graduate School of

The University of Texas at Austin

in Partial Fulfillment

of the Requirements

for the Degree of

Master of Arts

The University of Texas at Austin

December 2017

Dedication

The work in this thesis is dedicated to my family. From humble beginnings, we rise.

Acknowledgements

I would like to thank Dr. Jonathan Sessler for giving me the opportunity to work in his lab. Without Dr. Sessler's support, I would not have made it this far in my scientific career. I would also like to thank my fellow group members for all of the help I have received in lab, especially Dr. Gregory Thiabaud who helped me get established when I first joined the lab and started working with texaphyrin.

A special thank you is in order for the collaborators mentioned in this thesis. Dr. Peter Harvey of MIT and Dr. Brian Dolinar of Texas A&M, your interests in texaphyrin have allowed me to explore new areas of research. I would also like to thank Pharmacyclics, Inc. for providing the Sessler group with a surplus of Motexafin gadolinium, which was used by the author to produce the bis- and mono-amine functionalized derivatives of Motexafin gadolinium mentioned in this thesis.

Thank you to my family for always supporting my life's endeavors. To all of the mentors I have had along the way, thank you for sharing your wisdom with me. Finally, I would like to thank Joshua Avila for making Austin feel like home. Your love and support has given me the confidence to persevere through life's greatest adversities.

Abstract

New Developments in Texaphyrin Chemistry

Julie Alaniz, MA Chemistry

The University of Texas at Austin, 2017

Supervisor: Jonathan Sessler

Dr. Sessler et al. first synthesized Texaphyrin in the 1980s. Since then, this expanded porphyrin has been at the forefront of the Sessler group's research. Although decades worth of effort has been devoted to exploring texaphyrin and its derivatives, there still remain unexplored avenues of research related to the unique properties of this macrocyclic ligand. The work detailed in this thesis reflects an attempt to bring a fresh look into the world of texaphyrin chemistry. Chapter 1 of this thesis briefly delves into the background of texaphyrin. In Chapter 2, the synthesis of an MRI (magnetic resonance imaging) active derivative of texaphyrin is detailed. In Chapter 3, is discussed the synthesis and characterization of a Dy(III)-texaphyrin derivative that was studied for its potential as a single molecule magnet (SMM). Chapter 4 focuses on trying to improve the toxicity of well-known anticancer compounds through co-incubation with MGd, while Chapter 5 details the synthetic attempts to prepare a new Pt(II)-based Gd(III)-texaphyrin anticancer conjugate.

Table of Contents

List of Tables ix

List of Figures x

Chapter 1 Introduction: Texaphryin as a bioactive anticancer agent 1

Chapter 2 Synthesis of the bis-amine derivative of MGd for MRI applications 7

2.1 Introduction 7

2.2 Synthesis of bis-amine MGd 9

2.3 Conclusion 11

2.4 References 13

Chapter 3 Dysprosium-texaphyrin and its potential as a single molecule magnet 14

3.1 Introduction 14

3.2 Experimental 18

3.3 Conclusion 22

3.4 References 22

Chapter 4 *In vitro* studies of MGd co-incubated with Dp44mT 24

4.1 Introduction 24

4.2 *In vitro* studies 26

4.3 Conclusion 29

4.4 References 29

Chapter 5 The synthesis of new anticancer conjugates based on the MGd scaffold 31

5.1 Introduction 31

5.2 Synthesis of ethylenediamine monoacetic acid 34

5.3 Synthesis of [Pt(phen)Cl_2] 35

5.4 Synthesis of [Pt(phen)(EDMA)]Cl_2 35

5.5 Synthetic attempts for the desired anticancer conjugate 37

5.6 Conclusion 42

5.7 References 42

Chapter 6 Supplementary Data 44

References 52

List of Tables

Table 4.1: The 3-day IC_{50} values against the A549 cell line for Dp44mT, Dp44mT+100 μM MGd, Dp44mT+50 μM MGd, and Dp44mT+25 μM MGd. …… 28

List of Figures

Figure 1.1: Texaphyrin in its reduced, non-aromatic form (Tex1). Reagents for the indicated reactions: i. For Tex2 (metal-free form): air-saturated methanol/chloroform containing N,N,N'-tetramethyl-1,8-diaminonaphthalene ii. $CdCl_2$ with stirring for 24 hours in a methanol/chloroform air-saturated solution (to give Tex3) iii. Same procedure as in the case of ii, except $Cd(NO_3)_2$ was used as the metal source. Addition of excess pyridine then gives Tex4. 1

Figure 1.2: Metallation of the reduced form of texaphyrin concurrent with air-based oxidation. i) Reaction conditions include dissolving the reduced form of texaphyrin in methanol, followed by addition of 1.5-2 equivalents of the appropriate metal salt and an excess of dry triethylamine. The contents of the reaction flask are left open to the atmosphere and allowed to react overnight to afford a dark green solid. 2

Figure 1.3: The synthesis of cisPt^{IV}-TEX. 5

Figure 2.1: The synthesis of the bis- and mono-amine derivatives of MGd. 9

Figure 2.2: HPLC chromatogram monitored at 470 nm of the crude reaction mixture resulting from the conversion of MGd to the mono- and bis- amine derivatives, following the scheme in Figure 2.1. 10

Figure 2.3: The HPLC chromatograms of the purified bis-amine MGd product as monitored at 254, 420, 740, and 470 nm (from top to bottom). The intense peak at 6.4 min. corresponds to the bis-amine product. 12

Figure 2.4: The high-resolution ESI-MS report for the bis-amine product as generated by the Agilent Mass Spectrometer system. 12

Figure 3.1: A representative diagram of the electronic ground state of a Dy^{3+} ion,

following perturbation caused by spin-orbit effects. 15

Figure 3.2: Structure of a Dy-Tex complex containing two diphenyl phosphonate ligands in the axial positions. This structure is represented as [Dy-Tex(DPP)$_2$]. 16

Figure 3.3: The high-resolution ESI-MS for [Dy-Tex(NO_3)$_2$] at 803 m/z, which corresponds to $[M+CH_3O^-]^+$. In this case M = Dy(III)$C_{36}H_{42}N_5O_4$. Report generated from the Agilent mass spectrometer system. 20

Figure 3.4: The HPLC results for purified [Dy-Tex(NO_3)$_2$]. From top to bottom, the wavelengths monitored were 254, 420, 740, and 470 nm. 20

Figure 4.1: Structures of DpC and Dp44mT. 25

Figure 5.1: Structure of the MGd-PtInter1 conjugate synthesized in this study. 31

Figure 5.2: Synthetic scheme for the synthesis of [Pt(phen)(EDMA)]Cl_2. 34

Figure 5.3: UV-vis absorbance spectrum of 1,10-phen (red) in phosphate buffered saline, with HCl added to help dissolution. Also shown is the absorbance spectrum of [Pt(phen)(EDMA)]Cl_2 (blue). A Cary 5000 UV-vis-NIR spectrometer was used for these measurements. 36

Figure 5.4: ^{1}H NMR (400 MHz, D_2O) spectrum of [Pt(phen)(EDMA)]Cl_2. δ = 8.72 (4H, m), 7.96 (2H, s), 7.84 (2H, m), 3.67 (2H, appt dd, J = 86.1, J = 17.3), 3.05 (2H, appt dtd, J = 45.4, J = 13.35, J = 4.01), 2.72 (2H, appt dd, J = 54.01, J = 4.01). 37

Figure 5.5: Attempted syntheses of MGd-PtInter1. EDC HCl = N-(3-dimethylaminopropyl)-N'-ethylcarbodiimide hydrochloride, NHS = N-hydroxy succinimide, TEA = triethylamine 38

Figure 5.6: Partial RP-HPLC chromatogram of the reaction mixture of [Pt(phen)(EDMA)]Cl_2 and mono-amine MGd, after reacting in the presence of 1,1'-

carbonyldiimidazole. Wavelengths monitored include 254 nm (black), 275 nm (blue), 740 nm (pink), and 470 nm (brown). 39

Figure 5.7: Partial RP-HPLC chromatogram for the crude reaction mixture between [Pt(phen)(EDMA)]Cl_2 and mono-amine MGd as observed after reaction with EDC HCI and NHS coupling agents. Wavelengths monitored include 470 nm (brown), 740 nm (pink), 275 nm (blue), and 254 nm (black). 41

Figure 6.1 Logistic Fit of cell viability data for A549 cells incubated with Dp44mT (80-1.25 nM) over a 3-day period. Data was normalized to the control (cells incubated without Dp44mT). 44

Figure 6.2 Logistic Fit of cell viability data for A549 cells incubated with Dp44mT (80-1.25 nM) over a 3-day period. Data was normalized to the control (cells incubated without Dp44mT). 44

Figure 6.3 Logistic Fit of cell viability data for A549 cells incubated with Dp44mT (80-1.25 nM) over a 3-day period. Data was normalized to the control (cells incubated without Dp44mT). A = nM concentration of Dp44mT B = % viability 45

Figure 6.4 Logistic Fit of cell viability data for A549 cells incubated with Dp44mT+100 μM MGd over a 3-day period. Data was normalized to the control (cells incubated without Dp44mT/MGd). Concentration range of Dp44mT: 80-1.25 nM. 45

Figure 6.5 Logistic Fit of cell viability data for A549 cells incubated with Dp44mT+100 μM MGd over a 3-day period. Data was normalized to the control (cells incubated without Dp44mT/MGd). Concentration range of Dp44mT: 80-1.25 nM. 46

Figure 6.6 Logistic Fit of cell viability data for A549 cells incubated with Dp44mT+100 μM MGd over a 3-day period. Data was normalized to the control (cells incubated without

Dp44mT/MGd). Concentration range of Dp44mT: 80-1.25 nM. 46

Figure 6.7 Logistic Fit of cell viability data for A549 cells incubated with Dp44mT (80-1.25 nM) over a 3-day period. Data was normalized to the control (cells incubated without Dp44mT). 47

Figure 6.8 Logistic Fit of cell viability data for A549 cells incubated with Dp44mT (80-1.25 nM) over a 3-day period. Data was normalized to the control (cells incubated without Dp44mT). 47

Figure 6.9 Logistic Fit of cell viability data for A549 cells incubated with Dp44mT (80-1.25 nM) over a 3-day period. Data was normalized to the control (cells incubated without Dp44mT). 48

Figure 6.10 Logistic Fit of cell viability data for A549 cells incubated with Dp44mT+50 μM MGd over a 3-day period. Data was normalized to the control (cells incubated without Dp44mT/MGd). Concentration range of Dp44mT: 80-1.25 nM. 48

Figure 6.11 Logistic Fit of cell viability data for A549 cells incubated with Dp44mT+50 μM MGd over a 3-day period. Data was normalized to the control (cells incubated without Dp44mT/MGd). Concentration range of Dp44mT: 80-1.25 nM. 49

Figure 6.12 Logistic Fit of cell viability data for A549 cells incubated with Dp44mT+50 μM MGd over a 3-day period. Data was normalized to the control (cells incubated without Dp44mT/MGd). Concentration range of Dp44mT: 80-1.25 nM. 49

Figure 6.13 Logistic Fit of cell viability data for A549 cells incubated with Dp44mT+25 μM MGd over a 3-day period. Data was normalized to the control (cells incubated without Dp44mT/MGd). Concentration range of Dp44mT: 80-1.25 nM. 50

Figure 6.14 Logistic Fit of cell viability data for A549 cells incubated with Dp44mT+25 μM

MGd over a 3-day period. Data was normalized to the control (cells incubated without Dp44mT/MGd). Concentration range of Dp44mT: 80-1.25 nM. 50

Figure 6.15 Logistic Fit of cell viability data for A549 cells incubated with Dp44mT+25 μM MGd over a 3-day period. Data was normalized to the control (cells incubated without Dp44mT/MGd). Concentration range of Dp44mT: 80-1.25 nM. 51

Chapter 1: *Introduction: Texaphyrin as a bioactive anticancer agent*

The main focus of this thesis is lanthanide texaphyrin complexes and their conjugates. Texaphyrin is a Schiff base macrocycle of the expanded porphyrin variety. In its reduced form (Figure 1.1), texaphyrin is not an efficient ligand for cations. One of the first texaphyrin metal complexes was reported in 1988 by Sessler et al. and contained a coordinated Cd^{2+} metal center.[1] Upon oxidation of texaphyrin, the macrocycle becomes aromatic, with 22 electrons in the pi system. Normally, the oxidation of texaphyrin and its subsequent metal complexation are carried out simultaneously. The non-metallated

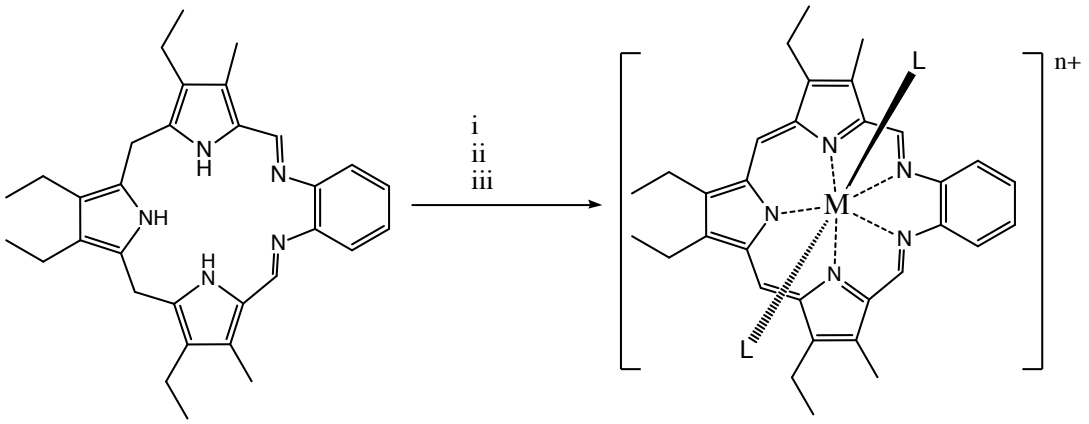

Figure 1.1 Shown on the left is texaphyrin in its reduced, non-aromatic form (Tex1). Reagents for the indicated reactions: i. For Tex2 (metal-free form): air-saturated methanol/chloroform containing N,N,N'-tetramethyl-1,8-diaminonaphthalene ii. $CdCl_2$ with stirring for 24 hours in a methanol/chloroform air-saturated solution (to give Tex3) iii. Same procedure as in the case of ii, except $Cd(NO_3)_2$ was used as the metal source. Addition of excess pyridine then gives Tex4.[1]

aromatic derivative of texaphyrin was isolated as its PF_6^- salt and was found to be relatively stable in the solid state and in acetonitrile. However, the macrocycle was found to decompose back to its reduced form in the presence of alcohols, alkylamines, and most other organic solvents.[2] This led to the suggestion that there is a high thermodynamic

benefit associated with metal complexation in the case of the oxidized texaphyrins, as complexation maintains the aromaticity of the ligand. Due to the instability of the texaphyrin core in its uncomplexed form, no binding constants have been determined for any of the metal complexes synthesized to date. The early texaphyrin systems were generally not soluble in water. Therefore, relatively early on an effort was made to improve their solubility. As a result of these efforts, it was found that the pegylated texaphyrin (Motexafin, Figure 1.2) forms aqueous stable complexes with lanthanides. These are moderately water soluble, a feature that is pivotal with regard to its complexes of Gd^{3+} and Lu^{3+}. (Figure 1.2) The focus of this thesis is complex 1 in Figure 1.2, referred herein as Motexafin Gadolinium (MGd).

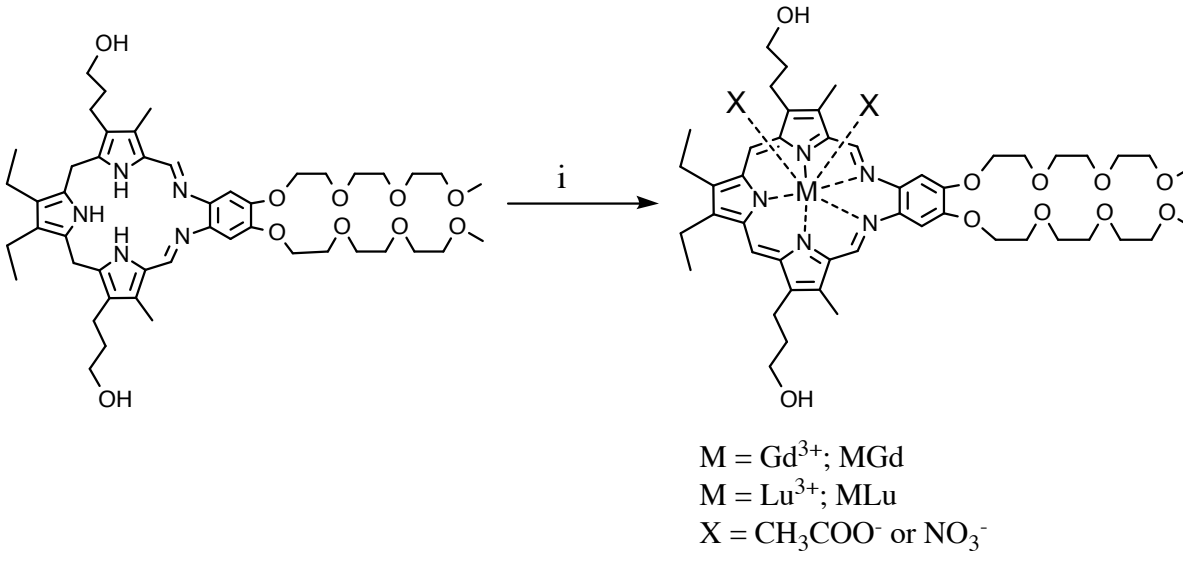

Figure 1.2 Metallation of the reduced form of texaphyrin concurrent with air-based oxidation. i) Reaction conditions include dissolving the reduced form of texaphyrin in methanol, followed by addition of 1.5-2 equivalents of the appropriate metal salt and an excess of dry triethylamine. The contents of the reaction flask are left open to the atmosphere and allowed to react overnight to afford a dark green solid.

The literature is abound with coordination complexes of Gd^{3+}, especially those used for magnetic resonance imaging (MRI) applications.[3,4] However, texaphyrin is unique in

that the core of MGd is bioactive, whereas most Gd^{3+} chelates are biologically inert. Early on, the biological properties of MGd were studied. Since the core of Motexafin can be described as an expanded porphyrin, it was rationalized that Motexafin should have interesting biological properties, as heme is a common motif in biological systems. It was soon discovered that MGd accumulates preferentially in cancerous tissue over normal tissue and promotes so-called redox cycling.[5,6] Since metallated texaphyrin is aromatic and contains a highly conjugated and delocalized pi system, the lowest unoccupied molecular orbital (LUMO) is relatively low in energy compared to traditional porphyrin systems. One consequence is that metallotexaphyrins are more readily reduced than their porphyrin counterparts.[7] Texaphyrin was found to show promise as a radiation sensitizer, and this key property was attributed to the ability of MGd to undergo a one-electron reduction in the presence of reducing metabolites, such as ascorbate and reduced glutathione.[6,8] *In vitro* experiments were performed that provide support for a mechanism of action *in vivo* that involves the one-electron reduction of MGd to $MGd^{\bullet-}$ by a reducing metabolite, followed by electron transfer to O_2 to form superoxide.[8,9] Superoxide is a highly reactive species that is quickly transformed to hydrogen peroxide *in vivo*, and the buildup of hydrogen peroxide in the cell can trigger apoptosis.[6] The ability of MGd to redox cycle and localize within cancerous tissue was one of the reasons it was explored as a radiation sensitizer.

Since MGd is bioactive and relatively well tolerated *in vivo*[10], a research theme in the Sessler Group has involved appending potent anticancer drugs to the MGd core *via* a covalent linker, so as to selectively deliver the drug to cancer cells.[11,12,13] One of the most prominent examples involves the appendage of a platinum based pro-drug ($cisPt^{IV}$-TEX) to the amine functionalized MGd core through amide coupling.[13] (Figure 1.3) $CisPt^{IV}$-TEX was

shown to be an active anticancer agent against the A2780 cell line, with an IC_{50} (half maximal inhibitory concentration) value of 1.28 μM.[13] This and a similar MGd derivative with an oxaliplatin subunit (oxaliPt^{IV}-TEX) are currently undergoing extensive evaluation for possible development as anticancer agents.[14] The work in this thesis is more focused on the science of texaphyrin. Chapters 2-3 detail the synthesis and characterization of two texaphyrin derivatives used in collaborative studies. Chapter 2 focuses on the bis-amine derivative of MGd and its potential use as an MRI contrast agent. Chapter 3 discusses a dysprosium-texaphyrin derivative and its magnetic properties. Chapters 4-5 are focused on research that is the exclusive work product of the author. Chapter 4 is concerned with *in vitro* studies on the A549 (lung carcinoma) cell line. Drug combination studies involving the use of MGd in conjunction with Dp44mT[15], a redox cycling anticancer drug, are presented. This work was carried out to determine whether or not a synergistic anticancer relationship exists between the two compounds in question. Chapter 5 focuses on the synthesis of a novel chemotherapeutic that utilizes MGd as a vessel for the targeted delivery of a well-known platinum-based DNA intercalator, $[Pt(phen)(en)]Cl_2$.[16]

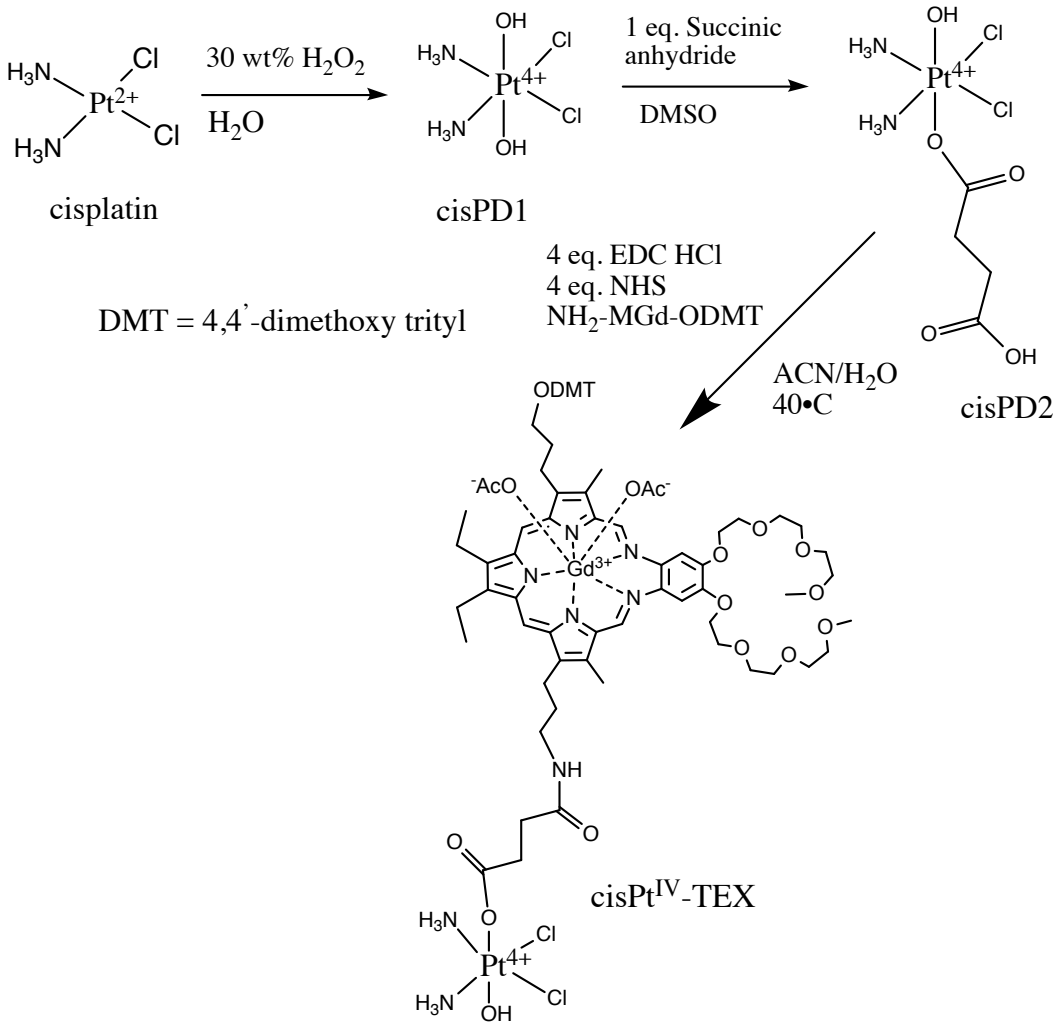

Figure 1.3 The synthesis of cisPt^{IV}-TEX.[13]

References

[1] Sessler, J. L. Murai, T. Lynch, V. Cyr, M. *J. Am. Chem. Soc.*, **1988**, 110, 5586-5588.

[2] Hannah S. Lynch, V. M. Gerasimchuk, N. Magda, D. Sessler, J. L. *Org. Lett.*, **2001**, 3, 3911-3914.

[3] Zhou, Z. and Lu, Z. *Wiley Interdiscip Rev Nanomed Nanobiotechnol.*, **2013**, 5, 1-18.

[4] Idee, J. Port, M. Raynal, I. Schaefer, M. Greneur, S. Corot, C. *Fundamental and Clinical Pharmacology*, **2006**, 20, 563-576.

[5] Arambula, J. F. Preihs, C. Borthwick, D. Magda, D. Sessler, J. L. *Anticancer Agents Med Chem.*, **2011**, 11, 222-232.

[6] Preihs, C. Arambula, J. F. Magda, D. Jeong, H. Yoo, D. Cheon, J. Siddik, Z. H. Sessler, J. L. *Inorg. Chem.*, **2013**, 52, 12184-12192.
[7] Sessler, J. L. Tvermoes, N. A. Guldi, D. M. Mody T. D. Allen, W. E. *J. Phys. Chem. A.*, **1999**, 103, 787-794.
[8] Magda, D. Gerasimchuk, N. Lecane, P. Miller, R. A. Biaglow, J. E. Sessler, J. L. *Chem. Commun.*, **2002**, 2730-2731.
[9] Sessler, J. L. Tvermoes, N. A. Guldi, D. M. Hug, G. L. Mody, T. D. Magda, D. *J. Phys. Chem. B*, **2001**, 105, 1452-1457.
[10] Meyers, C. A. Smith, J. A. Bezjak, A. Mehta, M. P. Liebmann, J. Illidge, T. Kunkler, I. Caudrelier, J. Eisenberg, P. D. Meerwaldt, J. Siemers, C. C. Gaspar, L. E. Curran, W. Phan, S. Miller, R. A. Renschler, M. F. *Journal of Clinical Oncology*, **2004**, 22, 157-165.
[11] Lee, M. H. Kim, E. Lee, H. Park, S. Y. Hong, K. S. Kim, J. S. Sessler, J. L. *Chem. Commun.*, **2016**, 52, 10551-10554.
[12] Wei, W. Fountain, M. E. Sessler, J. L. Magda, D. J. Wang, Z. Miller, R. A. *Macrocyclic Chemistry: Current Trends and Future Perspectives*, 407-425.
[13] Thiabaud, G. Arambula, J. F. Siddik, Z. H. Sessler, J. L. *Chem. Eur. J.*, **2014**, 20, 8942-8947.
[14] Sessler, J. L. Arambula, J. Siddik, Z. H. Thiabaud, G. Texaphyrin-pt(iv) conjugates and compositions for use in overcoming platinum resistance. US20170246182A1, Jun 11, 2014.
[15] Lovejoy, D. B. Sharp, D. M. Seebacher, N. Obeidy, P. Prichard, T. Stefani, C. Basha, M. T. Sharpe, P. C. Jansson, P. J. Kalinowski, D. S. Bernhardt, P. V. Richardson, D. R. *Journal of Medicinal Chemistry*, **2012**, 55, 7230-7244.
[16] Lippard, S. J. *Acc. Chem. Res.*, **1978**, 11, 211-217.

Chapter 2: *Synthesis of the bis-amine derivative of MGd for MRI applications*

2.1 Introduction

The literature is teeming with coordination complexes of Gd^{3+}, especially those used for magnetic resonance imaging (MRI) applications.[1] Arguably the most common macrocyclic chelate for gadolinium is DOTA (tetraazacyclododecane-1,4,7,10-tetraacetic acid) and its derivatives. Gadolinium complexes of DOTA are generally water-soluble and thermodynamically stable.[2] However, the macrocyclic core does not endow the complex with any ancillary properties. This is in contrast to Motexafin that shows tumor localization in many instances. The metal center of MGd is paramagnetic (Gd^{3+}=[Xe]$4f^7$). With its large magnetic moment and symmetrical distribution of unpaired electrons around the metal center, Gd^{3+} is the optimal metal for MRI signal enhancement.[3] Briefly, MRI is dependent on the relaxation of water protons in biological media that are subject to a strong magnetic field. A paramagnetic metal center, such as Gd^{3+}, can cause the relaxation rate of a proton within a given magnetic field to be modulated. The result is that the longitudinal ($1/T_1$) and transverse ($1/T_2$) relaxation rates are both increased.[3] Gd^{3+}-based MRI contrast agents are known as positive contrast agents because they cause an increase in signal intensity that results in a preferential increase in the longitudinal relaxation rate relative to the transverse rate of nearby tissues.[3] The relaxation of water occurs through a dipolar mechanism that is largely dependent on the relaxation of proton spin through coupling to a nearby fluctuating magnetic dipole. A fluctuating magnetic dipole can result from the electronic relaxation of Gd^{3+} ($1/T_{1e}$), rotational diffusion of the complex, and exchange of water between the first and second coordination spheres of the complex.[4] A prerequisite

for an efficient Gd^{3+} based MRI contrast agent then is an open coordination site for water molecules, allowing free exchange between the first, second, and third coordination spheres of the complex. This in turn, ensures maximal contact between the paramagnetic metal center and the bulk water. Since free Gd^{3+} is toxic to humans, all clinical MRI contrast agents based on a Gd^{3+} metal center must have high thermodynamic (or kinetic) stability, so as to prevent decomplexation when administered to a patient.[2] Complexes of MGd are extremely stable in aqueous media and have open coordination sites that allow water molecules to interact with the paramagnetic metal center. It should thus come as no surprise that researchers have been interested in developing MGd as a clinical MRI contrast agent.

MGd has been shown in several studies to act as an MRI contrast agent.[5-8] In one prominent study, rats with gliomas were administered MGd, and T1-weighted MRI images were taken to determine whether MGd was sufficient to define tumor margins.[5] It was found that MGd is most efficient as an intracellular MRI contrast agent 15-30 minutes after administration.[5] Since MGd localizes preferentially within cancerous tissue, the authors of the study hypothesized that MGd could be applied in an *in vivo* surgical setting to allow for the resection of the tumor with minimal damage to healthy tissue.[5] Studies such as these give credence to the idea that MGd can act as a responsive MRI contrast agent because it enters the cell and readily relaxes the bulk protons of water, giving positive contrast in MRI images.

In light of the above findings, a collaborative effort with Dr. Peter Harvey of the Massachusetts Institute of Technology was established in which the author of this thesis prepared samples of the bis-amine derivative of MGd for development as a stimuli-

responsive MRI contrast agent. The n-isopropyl hydroxyl substituents of the MGd core can be readily transformed to a variety of functional groups. In this case, both n-isopropyl hydroxyl appendages are transformed to primary amines, which can then be further functionalized.

2.2 Synthesis of bis-amine MGd

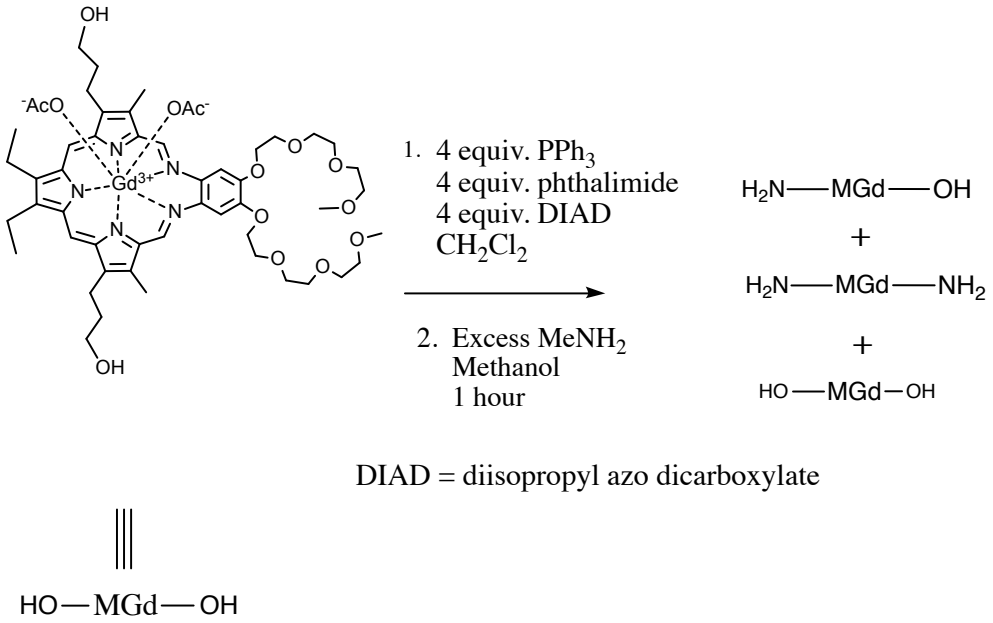

Figure 2.1 The synthesis of the bis- and mono-amine derivatives of MGd.[9]

The synthetic procedure of the desired intermediate is shown in Figure 2.2.1.[9] Under the reaction conditions in Figure 2.2.1, a statistical mixture of products is formed. Since the desired intermediate was the bis-amine MGd derivative, reaction times were optimized to get this as the major product. A 20-hour reaction time in the first step gives bis-amine functionalized MGd in almost exclusive yield, after amination with methylamine. Reverse-phase high performance liquid chromatography (RP-HPLC) was used to monitor the progression of the reaction. The HPLC system employed was a Thermo Scientific Dionex Ultimate 3000 outfitted with a photodiode array detector. The analytical column

used was a Thermo Scientific brand Syncronis C_{18} column (5 µM, 4.6 x 250 mm). The buffers used as the eluents were 0.1% acetic acid in high-purity water (eluent A), along with 0.1% acetic acid in acetonitrile (eluent B). The gradient began with 10% of eluent B, and increased to 99% eluent B over a 10-minute period. Four wavelengths were monitored (254, 420, 470, and 740 nm) that correspond to the signature UV-vis spectrum of MGd. A representative spectrum after amination with methylamine is show in Figure 2.2.2.

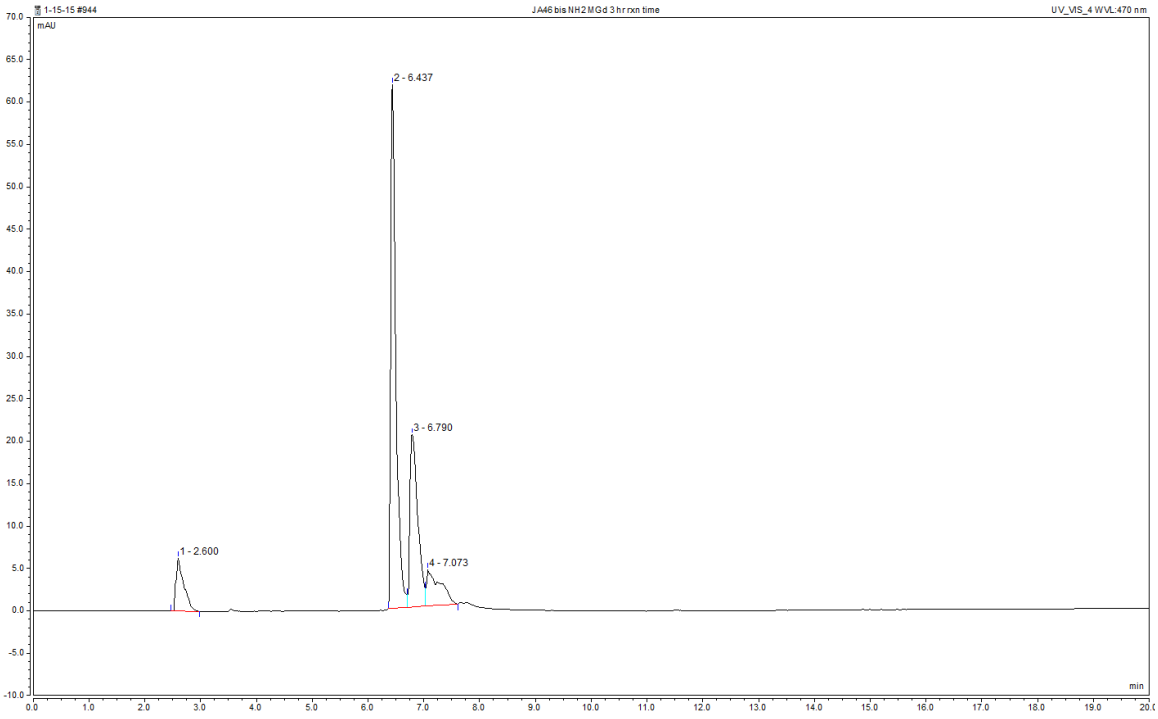

Figure 2.2 HPLC chromatogram monitored at 470 nm of the crude reaction mixture resulting from the conversion of MGd to the mono- and bis- amine derivatives, following the scheme in Figure 2.1. The large peak at 6.4 min. corresponds to desired bis-amine MGd. The middle peak at 6.8 min is the mono-amine derivative, and the peak at 7.2 min. is unreacted MGd.

After sufficient reaction with methylamine, the crude product mixture must be immediately loaded onto a reverse phase Sep-Pak tC_{18} column to remove excess methylamine. This is to avoid product degradation, as the basic conditions that methylamine produces can result in the degradation of MGd. After loading onto the column,

the crude mixture is flushed with ~2.5% acetonitrile in 0.1% acetic acid solution in water until all of the methylamine is removed. The bis-amine derivative comes off the column when the eluent consists of around 10-15% acetonitrile/0.1% acetic acid solution. In contrast, the mono-amine derivative elutes around 15-20% acetonitrile/0.1% acetic acid. Under these purification conditions, it is important to purify the products as quickly as possible, without compromising the quality of the separation, because product degradation increases with the time spent on the column. The HPLC chromatogram for the purified bis-amine MGd is shown in Figure 2.3.1. The absence of mono-amine MGd and MGd peaks at 6.8 and 7.2 min., respectively, indicates that the products can be separated from each other using reverse phase chromatography. The overall product yield for the bis-amine derivative under these conditions is ~35%. The low yield is due to complex degradation on the column, which cannot be avoided under the purification method used. High-resolution electrospray ionization mass spectrometry (ESI-MS) analyses were carried out at the University of Texas at Austin Mass Spectrometry Facility. The system used was an Agilent Technologies 6530 Accurate-Mass Q-TOF LC/MS. These studies served to confirm that the peak at 6.4 min. corresponds to the bis-amine derivative. This desired bis-amine product was detected as $[M\text{-}2OAc^-]^{2+}$ at 514 m/z. The high-resolution report is shown in Figure 2.3.2. Neither the mono-amine derivative or free MGd were observable in the MS data.

2.3 Conclusion

In conclusion, the conditions for the synthesis and purification of the bis-amine functionalized MGd are detailed. The final pure product was sent to Dr. Peter Harvey at MIT to test its MRI properties. While little feedback from Dr. Harvey has been received, it is believed that this MGd derivative will prove useful in making one or more stimuli-

responsive MRI contrast agents because MGd is readily taken up into cells and has already been established as providing positive contrast and enhanced signal in a clinical MRI setting.[5] The amine substituents of the bis-amine derivative can be further functionalized to introduce stimuli-responsive moieties, depending on the desired application. Dr. Peter Harvey is currently trying to develop such MRI active systems, using the bis-amine MGd derivative produced by the author.

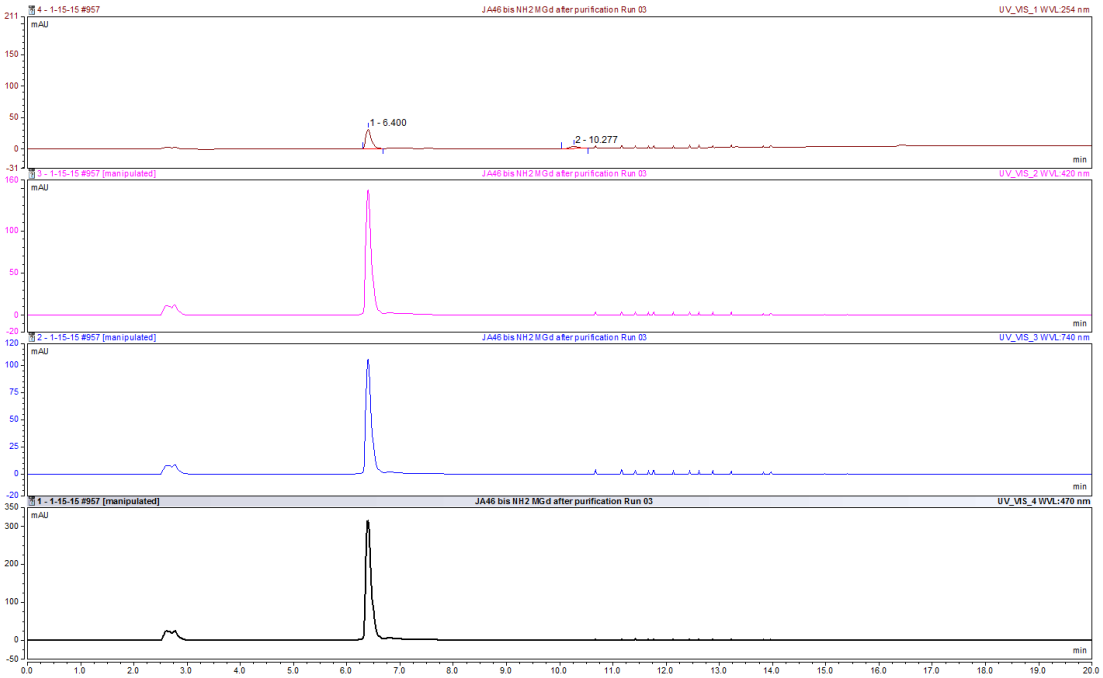

Figure 2.3 The HPLC chromatograms of the purified bis-amine MGd product as monitored at 254, 420, 740, and 470 nm (from top to bottom). The intense peak at 6.4 min. corresponds to the bis-amine product.

MS Spectrum Peak List

Obs. m/z	Calc. m/z	Charge	Abund	Formula	Ion/Isotope	Tgt Mass Error (ppm)
514.22080			434035.3			
1067.42570	1067.42980	1	1649.82	C49H69GdN7O10	M+	3.88
1070.43150	1070.43280	1	39127.47	C49H69GdN7O10	M+	1.16
1071.43270	1071.43330	1	74938.87	C49H69GdN7O10	M+	0.51
1072.43450	1072.43490	1	75995.92	C49H69GdN7O10	M+	0.35
1073.43530	1073.43530	1	97423.43	C49H69GdN7O10	M+	0.03
1074.43710	1074.43790	1	43928.85	C49H69GdN7O10	M+	0.72
1075.43760	1075.43780	1	67849.16	C49H69GdN7O10	M+	0.17
1076.43960	1076.44050	1	32290.84	C49H69GdN7O10	M+	0.81
1077.44210	1077.44320	1	9883.3	C49H69GdN7O10	M+	1.03

--- End Of Report ---

Figure 2.4 The high-resolution ESI-MS report for the bis-amine product as generated by the Agilent MS system.

2.4 References

[1] Zhou, Z. and Lu, Z. *Wiley Interdiscip Rev Nanomed Nanobiotechnol*., **2013**, 5, 1-18.

[2] Aime, S. Botta, M. Fasano, M. Terreno, E. *Chemical Society Reviews*, **1998**, 27, 19-29.

[3] Caravan, P. Ellison, J. J. McMurry, T. J. Lauffer, R. B. *Chem. Rev.*, **1999**, 99, 2293-2352.

[4] Caravan, P. *Chem. Soc. Rev.*, **2006**, 35, 512-523.

[5] Qiu, L. Zhang, F. Shi, Y. Bai, Z. Wang, J. Li, Y. Lee, D. Ingraham, C. Feng, X. Yang, X. *Radiology*, **2016**, 279, 400-409.

[6] Ford, J. M. Seiferheld, W. Alger, J. R. Wu, G. Endicott, T. J. Mehta, M. Curran, W. Phan, S. *International Journal of Radiation Oncology Biology Physics*, **2007**, 69 831-838.

[7] Manon, R. Hui, S. Chinnaiyan, P. Suh, J. Chang, E. Timmerman, R. Phan, S. Das, R. Mehta, M. *Technology in Cancer Research & Treatment*, **2004**, 3, 303-307.

[8] Hirschberg, H. Wu, G. N. Madsen, S. J. *Minim. Invasive Neurosurg.*, **2007**, 50, 318-323.

[9] Thiabaud, G. Arambula, J. F. Siddik, Z. H. Sessler, J. L. *Chem. Eur. J.*, **2014**, 20, 8942-8947.

Chapter 3: *Dysprosium-texaphyrin and its potential as a single molecule magnet.*

3.1 Introduction

Chapter 3 of this thesis details the synthesis and characterization of a dysprosium-texaphyrin derivative, which was studied on the basis of its potential single molecule magnet (SMM) behavior. Dysprosium is an *f*-block element with a ground state electronic configuration of [Xe]$4f^{10}6s^2$. It readily oxidizes to Dy^{3+} ([Xe]$4f^9$) to form stable complexes of high coordination number. In general, complex formation in lanthanides is largely electrostatically driven because the 4*f* subshell is very core-like and cannot readily interact with ligand orbitals.[1] In contrast to the third row transition metal series, spin-orbit coupling interactions dominate the spectroscopic and magnetic properties of the lanthanides.[1] This is largely due to the shielding of the 4*f* electrons by the 5*s* and 5*p* orbitals, which prevents interaction with the ligand field and leaves orbital angular momentum unquenched.[1] A common scheme used in the description of spin-orbit coupling is the Russel-Saunders term symbol. The Russel-Saunders ground state term symbol for the Dy^{3+} ion is $^6H_{15/2}$ ($^{2S+1}L_J$), which is the lowest energy electronic configuration for Dy^{3+}. This term arises from filling out the 4*f* orbitals of Dy^{3+}, according to Hund's rules.[1] In the case of lanthanides, spin-orbit coupling can break the degeneracy of the J states, which is the total angular momentum term given by L+S, L+S-1, …, |L-S|. (Figure 3.1.1) The crystal field can further split each individual J state, which has (2J + 1)-fold degeneracy, resulting in the magnetic substates of J (m_J). These arise from the asymmetry forced by the presence of the crystal field and are integer values of the following order: +J, J-1, …, -J.[1] Since the magnitude of spin-orbital interactions are relatively large for lanthanide ions, the excited J states are for the most part thermally inaccessible at room temperature, and so the ground state of

the ion dominates the magnetic properties.[1]

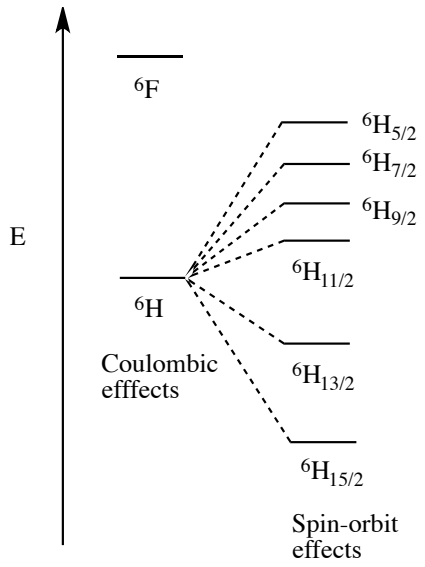

Figure 3.1 A representative diagram of the electronic ground state of a Dy^{3+} ion, following perturbation caused by spin-orbit effects.[2]

As a result of the large total angular momentum of the ground state Dy^{3+} ion, the effective magnetic moment of the free ion and its complexes are expected to be rather large, which makes Dy^{3+} a prime candidate for use in magnetic and spintronic applications. One such application that will be discussed herein is the possible use of dysprosium-texaphyrin (Dy-Tex; Figure 3.1.2) as a SMM. Single molecular magnetism occurs when a discrete molecular unit exhibits extremely slow magnetic relaxation times, such that magnetic hysteresis becomes significant and measurable.[2] This is desirable in the case of a SMM, since the system can retain its magnetization after removal of the magnetic field. To the extent this is true, an individual molecule can act as a memory storage device for a single byte of data. This could prove useful in relation to quantum computing.[2] However, most SMMs only exhibit magnetic hysteresis at extremely low temperatures (i.e. a few Kelvin).[3] The first SMMs synthesized and characterized were the Mn-based clusters $[Mn_{12}O_{12}(O_2CPh)_{16}(H_2O)_4]$ and $[Mn_{12}O_{12}(O_2CMe)_{16}(H_2O)_4]\bullet MeCOOH\bullet 3H_2O$ in 1993.[4] Much

of the current research in the field of SMM is focused on transition metal clusters. However, with the discovery that phthalocyanine based lanthanide sandwich complexes of D_{4d} symmetry exhibit exceptional SMM character,[5] complexes of lanthanides have since garnered much attention as SMMs.

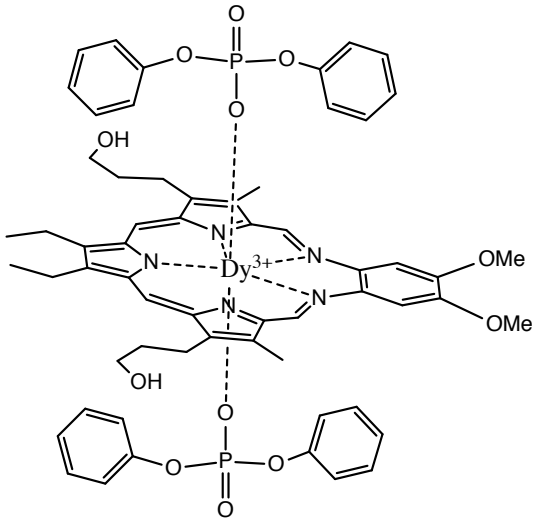

Figure 3.2 Structure of a Dy-Tex complex containing two diphenyl phosphonate ligands in the axial positions. This structure is represented as [Dy-Tex(DPP)$_2$].

A simple but effective structure-activity relationship for lanthanide SMMs was established by review of the electronic anisotropy of the metal center in relation to the ligand field environment.[2] Since Dy^{3+} has an electronic configuration of [Xe]$4f^9$, as the result of filling up the 4*f* orbitals according to Hund's rule, the metal ion is typically characterized by an uneven occupancy of the 4*f* subshell in favor of equatorial occupation. The shape of the quadrupole for a Dy^{3+} ion can thus be described as oblate.[2] The introduction of a coordination environment splits the m_J degeneracy, and so the projections of J will no longer be equal in energy.[3] For a complex to exhibit good SMM properties, the m_J projection with the largest magnitude should be the ground state configuration. Since Dy^{3+} is a Kramers ion, the ± degeneracy of a m_J state will not split in the absence of a magnetic

field.[3] In the case of a highly symmetric and homoleptic coordination environment, strong axial ligation with weak to no equatorial ligation maximizes m_J and, as a result, the magnetic anisotropy of the Dy^{3+} metal ion.[2] This is largely based on the idea that the oblate metal ion anisotropy interacts less with a ligand field in the axial positions, such that the magnitude of the larger m_J state is stabilized. While this model generally holds well for a homoleptic ligand field environment of the D_{4d} variety, it does not efficiently predict the magnetic anisotropy of heteroleptic systems, such as Dy-Tex.

In the case of lower symmetry Dy^{3+} complexes defined by a heteroleptic ligand environment, it is difficult to predict whether or not a complex will exhibit SMM behavior without experimental data or in-depth theoretical calculations. However, recent evidence provides support for the suggestion that a local crystal field symmetry of D_{5h} for a Dy^{3+} ion can impart SMM behavior.[6,7,8] In one study, a series of dysprosium polyoxometalates with D_{5h} symmetry were synthesized to gain insight into the properties that are desirable for SMM behavior within a D_{5h} coordination environment.[7] Results of the study indicate that good SMM behavior is observed for D_{5h} complexes in which the main magnetic axis in the ground state is aligned axially, or along the principal rotation axis. Further, within the D_{5h} environment studied, SMM is more pronounced when negatively charged ligands are in the axial position.[7] As there are not many examples of mononuclear Dy^{3+} complexes with D_{5h} symmetry that display SMM, it is worthwhile to study new systems, such as Dy-Tex, with similar local symmetry to see if the same trends hold.

Shown in Figure 3.1.2 is the Dy-Tex molecule studied in this thesis. The local symmetry is pseudo-D_{5h}, with strong axial ligation. In the equatorial plane, texaphyrin acts

as a pentacoordinate macrocycle, and in the axial position, there are two diphenyl phosphonate (DPP) ligands. Since the diphenyl phosphonate ligands bind through negatively charged oxygen atoms, the interaction with the Dy^{3+} center is presumably strong. As discussed above, lanthanides are hard Lewis acids and tend to favor interactions with hard Lewis bases. Testing whether [Dy-Tex$(DPP)_2$] can behave as a SMM was deemed worthwhile because recent evidence suggests that pentacoordinate ligation in the equatorial position coupled with strong axial coordination of a Dy^{3+} ion should produce a molecule with interesting magnetic properties.[7] Sessler et al. have studied the bulk magnetism of Motexafin ligated to Dy^{3+}. The magnetic moment was found to be 10.25±0.1 B.M., as measured in solution using the NMR method developed by Evans et al.[9] However, no study has looked at the SMM properties of any texaphyrin metal complex. Therefore, in collaboration with the Dunbar lab at Texas A&M, the SMM magnetism of Dy-Tex was studied. This thesis focuses on the synthesis, purification, and characterization of [Dy-Tex$(CH_3COO^-)_2$], [Dy-Tex$(NO_3^-)_2$], and [Dy-Tex$(DPP)_2$], whose general structures are shown in in Figure 3.1.2.

3.2 Experimental

Synthesis of [Dy-Tex$(NO_3^-)_2$]

The following procedure was used to synthesize a Dy-Tex complex with two nitrate counter ions instead of DPP (cf. Fig. 3.1.2). The methoxy version of texaphyrin (abbreviated as Tex in this thesis) was dissolved in methanol as its hydrochloride salt, and 1.5 equivalents of $Dy(NO_3)_3 \bullet 5H_2O$ were added to the reaction flask. The reaction was heated to reflux, and a slight excess of dry triethylamine was added, in order to deprotonate the texaphyrin ligand. The reaction was allowed to progress overnight. When the reaction was

deemed complete, the volatiles were removed under reduced pressure, and the dark green solid was dried further under vacuum to ensure removal of any remaining triethylamine.

The crude [Dy-Tex(NO_3)$_2$] product obtained above was loaded onto a neutral alumina column by dissolving the solid in a minimum amount of methanol and then diluting with dichloromethane. The crude material was then washed with 100% dichloromethane until most of the organic impurities were flushed off the column. A majority of the product was eluted using a 20% methanol/dichloromethane solution as the eluent. To maximize product yield, any Dy-Tex still on the column was eluted with 100% methanol. After this first purification, the resulting green solid was loaded onto a tC_{18} reverse phase Sep-Pak column developed by Waters Corporation. This was done by dissolving the solid in a minimum amount of acetonitrile and then diluting with 0.1 M KNO_3 in water. The product was eluted with 35% acetonitrile/0.1 M KNO_3. The product was then reloaded onto the Sep-Pak column and washed with HPLC grade water to remove any excess KNO_3 salt. The purified product was then eluted with 100% methanol, and the volatiles were removed under reduced pressure.

The reaction was performed on a one gram scale, with respect to the Tex hydrochloride salt, 500 mg of [Dy-OCH_3Tex(NO_3)$_2$] was obtained, which corresponds to a 36% yield. ESI-MS (positive mode) was used to confirm that the desired product was synthesized. In the low-resolution mode, the product was detected as $[M]^{2+}$ at 386, $[M+HCOO^-]^+$ at 817, and $[M+CH_3O^-]^+$ at 803 m/z, where M represents Dy(III)$C_{36}H_{42}N_5O_4$. The high-resolution spectrum at 803 is shown in Figure 3.2.1.

The purity of the product was determined using RP-HPLC. The same HPLC conditions as described in Chapter 2 were used. The wavelengths monitored were 254,

420, 470, and 740 nm. A representative HPLC spectrum is shown in Figure 3.2.2. The only

MS Spectrum Peak List

Obs. m/z	Calc. m/z	Charge	Abund	Formula	Ion/Isotope	Tgt Mass Error (ppm)
798.26250	798.26920	1	1442.84	C37H45DyN5O5	M+	8.41
799.26620	799.26670	1	12303.43	C37H45DyN5O5	M+	0.68
800.26780	800.26850	1	97331.54	C37H45DyN5O5	M+	0.96
801.26860	801.26910	1	172738.44	C37H45DyN5O5	M+	0.64
802.27050	802.27080	1	194303.99	C37H45DyN5O5	M+	0.36
803.27140	803.27160	1	212739.15	C37H45DyN5O5	M+	0.36
804.27340	804.27430	1	76844.53	C37H45DyN5O5	M+	1.16
805.27580	805.27710	1	16893.62	C37H45DyN5O5	M+	1.53
806.27640	806.27980	1	3083.32	C37H45DyN5O5	M+	4.22

--- End Of Report ---

Figure 3.3 The high-resolution ESI-MS for [Dy-Tex$(NO_3)_2$] at 803 m/z, which corresponds to $[M+CH_3O^-]^+$. In this case M = Dy(III)$C_{36}H_{42}N_5O_4$. Report generated from the Agilent MS system.

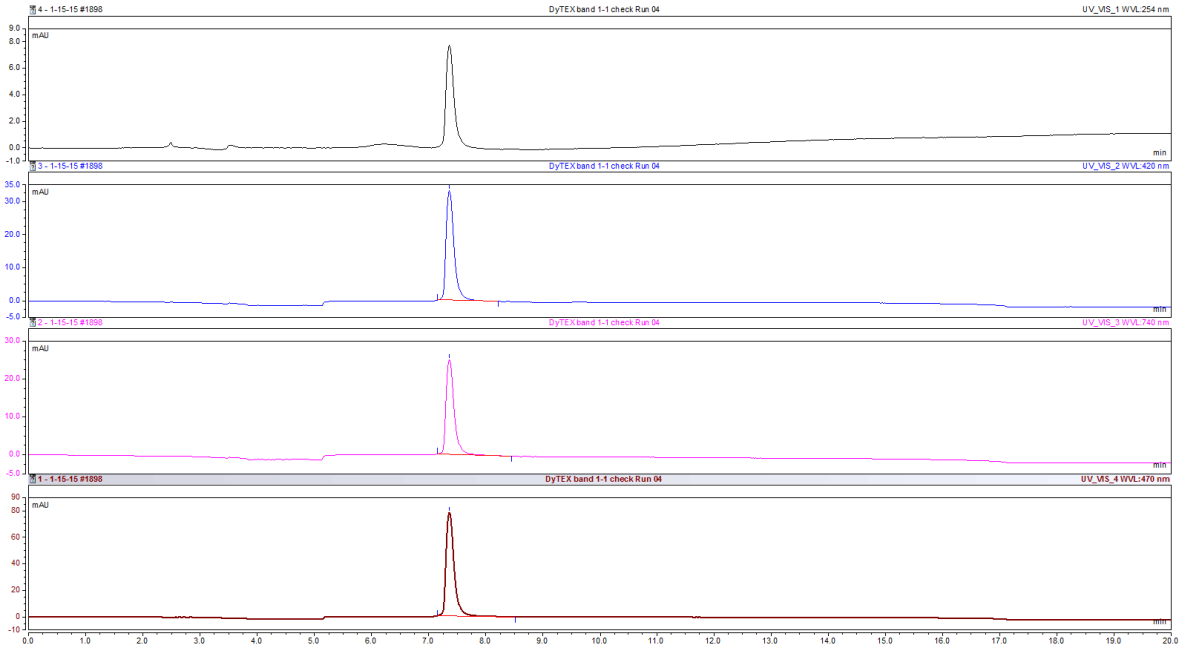

Figure 3.4 The HPLC results for purified [Dy-Tex$(NO_3)_2$]. From top to bottom, the wavelengths monitored were 254, 420, 740, and 470 nm.

peak observable at the wavelengths monitored was a sharp peak at 7.4 min. Based on this observation, the product was deemed to be sufficiently pure to allow magnetic studies to be performed. Several attempts were made to grow crystals of [Dy-Tex$(NO_3)_2$]. The methods used were slow evaporation of solvent, vapor diffusion, and layer deposition. However, no crystals of X-ray diffraction quality were obtained, regardless of the

conditions used to grow the crystals. While failure is always difficult to rationalize, it is possible that there may have been some excess KNO_3 present in the final product, which would interfere with the crystallization of [Dy-Tex$(NO_3)_2$]. Support for this comes from the observation of small, clear crystals that formed in preference to crystalline [Dy-Tex$(NO_3)_2$].

Synthesis of [Dy-Tex$(DPP)_2$]

The first reported synthesis of a dysprosium-texaphyrin derivative with two DPP counter ions ligated in the axial positions was by Mody et al. in 1995.[10] A similar procedure was followed to transform the [Dy-Tex$(NO_3)_2$] synthesized according to the above method into [Dy-Tex$(DPP)_2$]. Briefly, the [Dy-Tex$(NO_3)_2$] was dissolved in a minimum amount of a 1:1 mixture of methanol/dichloromethane. Then, 5 equivalents of the sodium salt of DPP were dissolved in a minimum amount of methanol, and this solution was layered on top of the [Dy-Tex$(NO_3)_2$] solution. The Dy-Tex was left in the dark over a seven-day period. The solid that had precipitated out of solution was collected through vacuum filtration and washed with methanol. The reaction was performed on a 50 mg scale, with respect to [Dy-Tex$(NO_3)_2$], and 27 mg of a green solid believed to be [Dy-Tex$(DPP)_2$] was obtained, corresponding to a 40% yield. However, this sample was sent to Atlantic Microlab, Inc. for C, H, N elemental analysis, and the results did not verify the purity of the [Dy-Tex$(DPP)_2$] sample. (Calculated: C: 56.76% H: 4.92% N: 5.52% Found: C: 51.12% H: 5.18% N: 7.42%) Further, single crystals of the final product could not be grown under the conditions tested. Since no conclusive evidence was obtained for the purity of the [Dy-Tex$(DPP)_2$] synthesized, the SMM behavior of this complex could not be tested. ESI-MS and HPLC alone are not sufficient characterization techniques for purity determination because anion exchange with the media can readily occur, resulting in inconclusive results. As a

minimum, X-ray diffraction data is needed to gain a full understanding of the SMM behavior.

Synthesis of [Dy-Tex(CH_3COO^-)$_2$]

The acetate version of Dy-Tex was synthesized in a manner similar to that detailed above for [Dy-Tex(NO_3^-)$_2$]. However, Dy(CH_3COO^-)$_3$ was used as the metal source, and during the reverse-phase purification step, acetonitrile/0.1 M $NH_4^+CH_3COO^-$ in water was used as the solvent system. The presence of the desired product was again confirmed by ESI-MS (positive mode), and the purity of the sample was established by HPLC. The reaction was performed on a one gram scale, and the purified product was obtained in 40% yield.

3.3 Conclusion

Dr. Brian Dolinar, a post-doc in the Dunbar Group, and the original initiator of this project, was able to test the [Dy-Tex(CH_3COO^-)$_2$] and [Dy-Tex(NO_3^-)$_2$] complexes for SMM activity. However, according to his results, no SMM behavior was observed for either complex (actual data not shown). Still, it is worth trying to isolate [Dy-Tex(DPP)$_2$] in pure form because the DPP counter ions should provide a higher local symmetry around the Dy^{3+} ion, which then might result in improved SMM behavior. Also, complexes of texaphyrin with other paramagnetic lanthanide cations should be made and tested for possible SMM behavior. This would allow a more comprehensive electronic structure-activity relationship to be obtained. The author is currently undertaking this work.

3.4 References

[1] Li, W. Zhou, G. Mak, T. C. W. *Advanced Structural Inorganic Chemistry*, Oxford University Press: New York, 2008; p 54-63 and 685-687.

[2] Rinehart, J. D. and Long, J. R. *Chem. Sci.*, **2011**, 2 2078-2085.

[3] Zhang, P. Gui, Y. Tang, J. *Coordination Chemistry Reviews*, **2013**, 257, 1728-1763.

[4] Sessoli, R. Tsai, H. L. Schake, A. R. Wang, S. Vincent, J. B. Folting, K. Gatteschi, D. Christou G. and Hendrickson, D. N. *J. Am. Chem. Soc.*, **1993**, 115, 1804–1816.

[5] Ishikawa, N. Sugita, M. Ishikawa, T. Koshihara, S. Kaizu, Y. *J. Am. Chem. Soc.*, **2003**, 125, 8694-8695.

[6] Chen, Y, Liu, J. Ungur, L. Liu, J. Li, Q. Wang, L. Ni, Z. Chibotaru, L. F. Chen, X. Tong, M. *J. Am. Chem. Soc.*, **2016**, 138, 2829-2837.

[7] Li, J. Yuan, C. Yang, L. Kong, M. Zhang, J. Ge, J. Zhang, Y. Song, Y. *Inorganic Chemistry*, **2017**, 56, 7835-7841.

[8] Gavey, E. L. Beldjoudi, Y. Rawson, J. M. Stamatatos, T. C. Pilkington, M. *Chem. Commun.*, **2014**, 50, 3741-3743.

[9] Guldi, D. M. Mody, T. D. Gerasimchuk, N. N. Magda, D. Sessler, J. L. *J. Am. Chem. Soc.*, **2000**, 122, 8289-8298.

[10] Lisowski, J. Sessler, J. L. Lynch, V. Mody, T. D. *J. Am. Chem. Soc.*, **1995**, 117, 2273-2285.

Chapter 4: *In vitro studies of MGd co-incubated with Dp44mT*

4.1 Introduction

Although MGd was tested early on as a possible radiation sensitizer and is an agent that is known to localize preferentially in cancerous cells, it is not particularly cytotoxic. Perhaps the main utility of this expanded porphyrin stems from its ability to redox cycle in biological milieus and to concentrate within neoplastic tissues.[1] To exploit these desirable attributes, efforts in the Sessler group have focused on attaching a known potent chemotherapeutic, such as doxorubicin or cisplain, to MGd via a covalent linker. The thinking is that the conjugate will allow a higher concentration of the cytotoxic drug to be delivered to the cancerous tissue.[2,3,4] The author's own efforts to develop such a conjugate will be detailed in a later chapter of this thesis. However, these putative MGd-based anticancer conjugates are often synthetically challenging to make. Therefore, a simpler strategy was revisited as detailed in this chapter. Briefly, an unmodified MGd is rationally paired with a potent chemotherapeutic with the goal of improving the efficacy of both species. A drug series that seems most promising in this regard is the di-2-pyridylketone thiosemicarbazone (DpT) ligand class. (Figure 4.1.1)

Thiosemicarbazones are a class of ligands that have long been studied for their interesting biological properties.[5] The main interest in this class within the context of this thesis lies in the fact that both DpC and Dp44mT, are highly potent.[6] These ligands can bind bioavailable transition metals, such as Fe(II) and Cu(II), in a tridentate fashion through N(pyridine), N(imine), S ligation.[7] The free ligands are actively transported into the cell through P-glycoprotein mediated endocytosis.[6] The ligands can be effluxed out of the cell, but a significant percentage is transported into the lysosome, through P-glycoprotein

receptors. The acidic pH of the lysosome protonates the ligand, effectively trapping it within the lysosome, where Dp44mT and DpC have been shown to bind available Cu and redox cycle.[6] Under these latter conditions, a buildup of harmful levels of ROS (reactive oxygen species) is seen. This can lead to lysosomal membrane permeability, which allows for drugs trapped within the lysosome to be released at their proposed off-target site.[6] A recent study showed a synergistic effect when Dp44mT or DpC and common chemotherapeutics, such as doxorubicin and cisplatin, are co-incubated with the A549 cell line.[7] The lysosomal targeting ability of Dp44mT and its pronounced redox activity are both features likely to be enhanced by the introduction of MGd into the system.

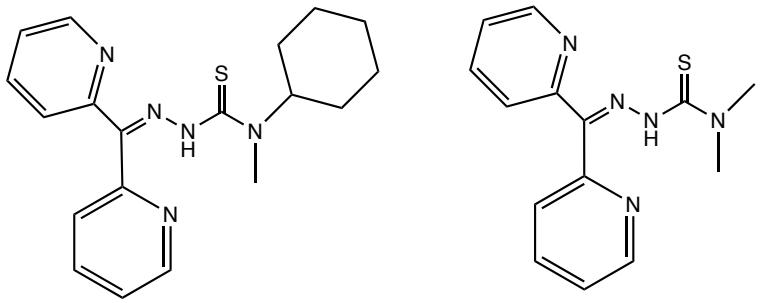

Figure 4.1 Structures of DpC and Dp44mT.[7]

MGd has been shown to concentrate preferentially within certain intracellular compartments, such as the lysosome and endoplasmic reticulum.[8] Since MGd also redox cycles within cells and localizes within the lysosome, it might be expected that the addition of a DpT ligand and MGd would have a synergistic anticancer effect against certain cancer cell lines. Tumor cells are especially sensitive to redox metabolism, so it is hypothesized that overwhelming of the antioxidant defense systems by over production of ROS will

trigger cell death.[9] Therefore, the goal of this chapter was to test whether the presence of MGd would decrease the IC_{50} value of Dp44mT against the A549 cell line.

Dp44mT has been studied extensively as the lead drug candidate of the DpT class for its high potency, but it has exhibited unwanted side effects, such as cardiotoxicity at high doses.[7] Therefore, DpC was developed to circumvent some of the problems observed with Dp44mT and is now the lead candidate of this drug series. Still, Dp44mT serves as a good *in vitro* model and was used in this study.

4.2 *In vitro* studies

MGd was co-incubated with Dp44mT at a constant concentration of 25, 50, and 100 μM, and the 3-day IC_{50} value of Dp44mT was measured, using the MTT (3-(4,5-dimethylthiazol-2-yl)-2,5-diphenyl tetrazolium bromide) colorimetric assay. An antagonistic effect would be established, if MGd significantly increased the IC_{50} of Dp44mT, as judged by Student's t-test. Conversely, a synergistic effect would be established if a significant decease in the IC_{50} of Dp44mT were observed. If no change in the IC_{50} value was seen, then it could be concluded that MGd did not have an appreciable effect on the efficacy of Dp44mT at the values tested.

Dp44mT was purchased from Alfa Aesar and used without further purification, while MGd was synthesized according to published procedures.[10] ESI-MS (positive mode) and RP-HPLC were used to verify that MGd was formed in high purity. The A549 cell line was cultured according to established procedures.[11] Briefly, the cells were grown in RPMI medium supplemented with 10% heat inactivated fetal bovine serum and antibiotics (streptomycin and penicillin). Cells were seeded in 96-well microliter plates at 1,500 cells per well and allowed to adhere overnight in the aforementioned medium, before

incubating with either Dp44mT or MGd, or both. Stock solutions of Dp44mT were prepared fresh in DMSO the day of injection. Final DMSO concentration in wells (v/v) did not exceed 0.5%. Serial dilutions (two-fold) from the stock solution of Dp44mT (40 μM) were prepared to give a final concentration in the wells ranging from 80-1.25 nM. MGd stock solutions were prepared in RPMI medium.

The general experimental set-up is detailed as follows. Cells incubated with Dp44mT only served as the positive control group. The average IC_{50} of each experimental group (cells incubated with 100 μM MGd/Dp44mT, 50 μM MGd/Dp44mT, and 25 μM MGd/Dp44mT) was compared to the positive control group. In order to prevent other variables (e.g. cell passage or growth conditions) from affecting the experimental outcome, the positive control and experimental group for each trial (three trials total for each experimental group) were incubated with drug concurrently. This is reflected in the data (Table 4.2.1). The positive control group for 50 μM MGd/Dp44mT and 25 μM MGd/Dp44mT is the same, as the trials for the positive control were performed concurrently with the experimental group. The trials for the positive control group for 100 μM MGd/Dp44mT were performed concurrently, but with different passages of the cell line than 50 μM MGd/Dp44mT and 25 μM MGd/Dp44mT.

The wells and culture flasks were kept in an incubator at 37°C and 5% CO_2. After a 3-day incubation period, 50 μL of a 3mg/mL stock solution of the MTT dye prepared in RPMI medium was added to each well. The plates were incubated for 2 more hours, after which each well was emptied of its contents, and the purple precipitate of the reduced dye was dissolved in 50 μL of DMSO. A microplate reader (ChroMate, Awareness Technologies Inc.) was used to read absorbance values at 570 nm. The absorbance values were

normalized to the control, which was cells incubated without drug. The data was fitted to a sigmoidal dose-response curve, calculated using the logistic function provided by OriginPro. The IC_{50} values given in Table 4.2.1 are the result of three trials involving consecutive passages of the cell line. The overall passage did not exceed 15. Dp44mT was used as the positive control. The published 3-day IC_{50} value for Dp44mT against the A549 cell line is 20±0.008 nM.[7] However, under the tested conditions this value (Table 4.2.1) proved lower. The corresponding data for the respective Dp44mT/MGd combinations is also given in Table 4.2.1. Logistic plots can be found in Ch. 6.

IC_{50}	Dp44mT	D44mT+100μM MGd	Dp44mT	Dp44mT+50μM MGd	Dp44mT+25μM MGd
Trial 1	6.89	6.31	11.49	10.52	10.23
Trial 2	7.26	6.89	13.47	12.44	11.54
Trial 3	8.35	8.91	11.96	11.11	16.78
Average	7.5	7.37	12.31	11.36	12.85
Std. Dev.	0.76	1.36	1.03	0.98	3.47

Table 4.1 The 3-day IC_{50} values against the A549 cell line for Dp44mT, Dp44mT+100 μM MGd, Dp44mT+50 μM MGd, and Dp44mT+25 μM MGd.

Student's t test at the 95% confidence interval was used to determine whether or not the positive control group (IC_{50} of Dp44mT) differed from the average IC_{50} of Dp44mT+MGd. The average IC_{50} value for Dp44mT+100 μM MGd was 7.37±1.36 nM, which proved comparable to the IC_{50} of the positive control (7.5±0.76 nM). In other words, the average IC_{50} values for the positive control and Dp44mT+100 μM MGd do not differ at the 95% confidence level. Similarly, comparing the average positive control IC_{50} (12.31±1.03 nM) to the average IC_{50} for Dp44mT+50 μM MGd (11.36±0.98 nM) confirmed that there is no statistically significant difference between the averages. Finally, comparing the average

IC_{50} for the positive control (12.31±1.03 nM) and Dp44mT+25 μM MGd (12.85±3.47) confirms that the averages do not differ.

4.3 Conclusion

The negative results of the *in vitro* assays were not expected, as the hypothesis was that MGd would sensitize the A549 cells to the toxicity of Dp44mT. One explanation for the negative results is that the A549 cell line is too insensitive to the effects of MGd (5 day IC_{50} > 100 μM)[11], such that even in the presence of an efficient ROS generator like Dp44mT, MGd has no effect on the redox metabolism of the cell. In this regard, it would be interesting to test the effect MGd has on the IC_{50} of Dp44mT on a cell line that is inherently more sensitive to the effects of MGd, such as the A2780 cell line (5 day IC_{50} > 70 μM).[11] The driving force for the completion of such studies is the idea that MGd can sensitize the tumor to the effects of a highly toxic anticancer drug, such that a lower dose of the drug can be administered to patients in a clinical setting, resulting in diminished off-target side effects.

4.4 References

[1] Preihs, C.; Magda, D. J.; Sessler, J. L. *Bioinorg React Mech.*, **2013**, 9, 3-14.
[2] Lee, M. H.; Kim, E.; Lee, H.; Park, S. Y.; Hong, K. S.; Kim, J. S.; Sessler, J. L. *Chem Comm.*, **2016**, 52, 10551-10554.
[3] Arambula, J. F.; Sessler, J. L.; Siddik, Z. H. *Medchemcomm*., **2012**, 3, 1275-1281.
[4] Thiabaud, G.; Arambula, J. F.; Siddik, Z. H.; Sessler, J. L. *Chem. Eur. J.*, **2014**, 20, 8942-8947.
[5] Yu, Y. Kalinowski, S. Kovacevic, Z. Siafakas, A. R. Jansson, P. J. Stefani, C. Lovejoy, D. B. Sharpe, P. C. Bernhardt, P. V. Richardson, D. R. *J. Med. Chem.*, **2009**, 52, 5271-5294.
[6] Seebacher, N. A.; Richardson, D. R.; Jansson, P. J. *Cell Death and Disease*, **2016**, 7, 1-13.
[7] Lovejoy, D. B.; Sharp, D. M.; Seebacher, N.; Obeidy, P.; Prichard, T.; Stefani, C.; Basha, M. T.l Sharpe, P. C.; Jansson, P. J.; Kalinowski, D. S.; Bernhardt, P. V.; Richardson, D. R. *Journal of Medicinal Chemistry*, **2012**, 55, 7230-7244.

[8] Woodburn, K. W. *The Journal of Pharmacology and Experimental Therapeutics*, **2001**, 297, 888-894.

[9] Kim, J. Kim, J. Bae, J. *Experimental and Molecular Medicine*, **2016**, 28, 1-13.

[10] Guldi, D. M. Mody, T. D. Gerasimchul, N. N. Magda, D. Sessler, J. L. *J. Am. Chem. Soc.*, **2000**, 122, 8289-8298.

[11] Thiabaud, G. McCall, R. He, G. Arambula, J. F. Siddik, Z. H. Sessler, J. L. *Angew. Chem. Int. Ed.*, **2016**, 55, 12626, 12631.

Chapter 5: *The synthesis of new anticancer conjugates based on the MGd scaffold.*

5.1 Introduction

Following the motif of covalently linking a known anticancer compound onto MGd, the derivative MGd-PtInter1 was designed and synthesized. (Figure 5.1.1) The new drug is based on the $[Pt(phen)(en)]Cl_2$ anticancer compound, which was first synthesized and characterized by Lippard et al. (phen = 1,10-phenanthroline, en = ethylenediamine).[1] $[Pt(phen)(en)]Cl_2$ is part of a class of compounds known as DNA intercalators. Intercalation of planar organic heteroaromatics between stacked DNA base pairs has been studied since the 1960s.[2] 1,10-Phenanthroline is the parent compound of a series of DNA intercalators. Since the strength of DNA intercalation relies heavily on π-π donor-acceptor interactions, traditional DNA intercalators are often based on highly aromatic organic dyes.[3] The main target for the $[Pt(phen)(en)]Cl_2$ intercalator is the minor groove of DNA. This is because the parent system displays high specificity for the intercalation sites defined by C_3-G_4 and T_2-A_5 base pairs.[4] Intercalation causes the unwinding, lengthening, and stiffening of double-stranded DNA, which has an overall cytotoxic effect.[4]

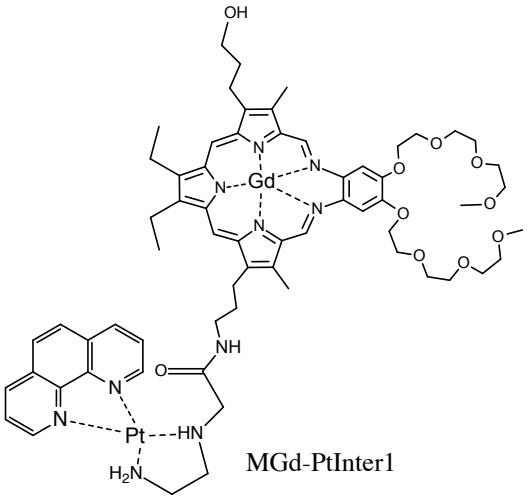

Figure 5.1 Structure of the MGd-PtInter1 conjugate synthesized in this study.

One drawback that is common with solely organic intercalators is that they have low solubility in aqueous solution. Thus, their utility in biological systems is limited. DNA intercalators based on metal complexes often have the advantage of increased water solubility over traditional organic dyes. Also, the metal center often imparts favorable properties to the intercalator, such as an ability to catalyze the production of ROS.[2] In the case of the $[Pt(phen)(en)]Cl_2$ system, the Pt^{2+} metal center serves to increase water solubility of the 1,10 phenanthroline intercalator, maintain a kinetically inert metal complex, and increase the overall positive charge of the intercalator. The latter feature serves to increase the affinity for DNA binding, as DNA has a negatively charged backbone.[4]

The typical structure of these types of complexes is represented as $[Pt(II)(I_L)(A_L)]Cl_2$, in which I_L is a bidentate intercalating ligand and A_L is typically a non-intercalating bidentate ancillary ligand.[4] Aldrich-Wright et al. analyzed over 60 such Pt compounds, all of which were based on derivatives of 1,10-phenanthroline (I_L) and various ancillary ligands. The complex with the most pronounced anticancer activity was $[$(5,6-dimethyl-1,10-phenanthroline)(1S,2S-diaminocyclohexane)$Pt(II)]^{2+}$, which displayed 100-fold greater toxicity than cisplatin in the L1210 murine leukemia cell line.[5] Although drugs of the type $[Pt(II)(I_L)(A_L)]Cl_2$ usually display high levels of antitumor activity, they often suffer from dose-limiting toxicity, as the complexes are not specific to cancerous tissue.[5] Therefore, this class of highly potent anticancer compounds might benefit from selective delivery of the agent to the tumor site.

Along these lines, a few studies have been published that involve the supramolecular encapsulation of the $[Pt(II)(I_L)(A_L)]Cl_2$ complexes within drug delivery vehicles, based on scaffolds such as cucurbit[6]uril[5], β-cyclodextrin and calix[4]arene.[6]

Cucurbit[6]uril was restricted as an efficient delivery vehicle, due to its low solubility in water.[5] The carboxylated-β-cyclodextrin and *p*-sulfonatocalix[4]arene proved to be much better hosts for selective delivery of the Pt intercalators, as they had improved water solubility, protected the complexes from degradation by reduced glutathione, and did not significantly decrease the *in vitro* cytotoxicity of the tested $[Pt(II)(I_L)(A_L)]Cl_2$.[6] Since there is an obvious need for the development of vehicles that can efficiently and selectively deliver Pt-based DNA intercalators, the work in this chapter of the thesis focuses on synthesizing novel anticancer conjugates based on the MGd scaffold.

The rationale for preparing the MGd-PtInter1 conjugate is the perceived benefit associated with being able to selectively deliver these highly toxic anticancer intercalators to cancerous lesions. As discussed in Chapter 1 of this thesis, MGd is a known biocompatible small molecule that localizes preferentially within certain cancerous tissues.[7] In the past, the Sessler group has synthesized Pt-based MGd anticancer conjugates as putative Pt drugs.[8,9] However, the Pt agents appended to MGd thus far have solely been of the cisplatin[8] and oxaliplatin[9] class. When the MGd pro-drug conjugates are reduced, cisplatin and oxaliplatin are released, which form dative adducts with nitrogenous base pairs of DNA[9], in particular at the N7 position of guanine.[10] The intercalative mechanism of action of $[Pt(phen)(en)]Cl_2$ is very different than the traditional cisplatin and oxaliplatin systems. Thus, the author felt it would be valuable to create a MGd derivative of a Pt-based intercalator and to test its DNA binding properties, cytotoxicity, cellular distribution within cells, and stability in an *in vitro* setting. Of course, the main determinant in the utility of the new anticancer conjugate is cytotoxicity. Such studies remain to be performed by the author. The purpose of this thesis chapter is to detail the optimal reaction conditions

developed for the synthesis of a previously unreported Pt anticancer conjugate $[Pt(phen)(EDMA)]Cl_2$ (EDMA = ethylenediamine monoacetic acid; Figure 5.1.2), along with the optimal reaction conditions for the synthesis of MGd-PtInter1. Unfortunately, the newly synthesized MGd-PtInter1 could not be isolated by the purification methods employed. The synthetic scheme for the synthesis of $[Pt(phen)(EDMA)]Cl_2$ is shown in Figure 5.1.2.

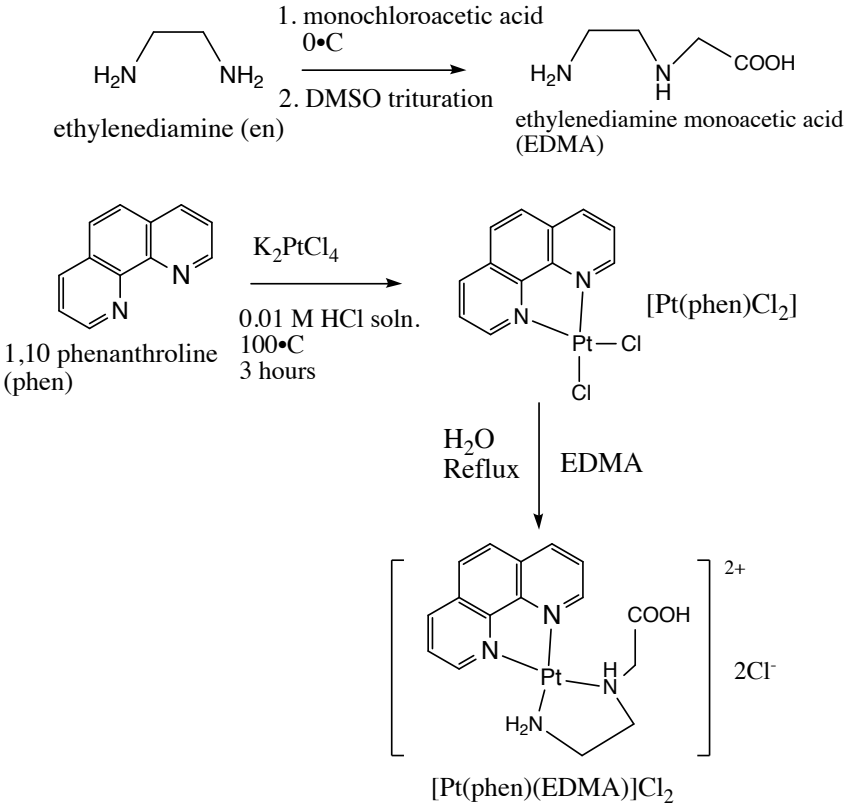

Figure 5.2 Synthetic scheme for the synthesis of $[Pt(phen)(EDMA)]Cl_2$.

5.2 Synthesis of ethylenediamine monoacetic acid

EDMA was synthesized according to a previously reported procedure.[11] The reaction was performed on a 1 gram scale with respect to monochloroacetic acid. After removing most of the unreacted en starting material under reduced pressure, ~40 mL of DMSO was added to the reaction mixture, which was left to sit overnight under light stirring. A white precipitate formed, which was filtered off and dried under vacuum to give

0.95 g of EDMA (~80% yield). No recrystallization was needed, as the product was deemed sufficiently pure by ^{1}H NMR spectroscopy to be carried on into the next step. The ^{1}H NMR (400 MHz, D_2O; Agilent MR 400) data for this material were as follows: 3.08 (s, 2H), 2.84 (app t, J = 6.36, 2H), 2.71 (app t, J = 6.36, 2H).

5.3 Synthesis of [Pt(phen)Cl_2]

After the EDMA ligand was synthesized, the [Pt(phen)Cl_2] complex was formed using a combination of established procedures.[12,13] Briefly, a slight excess (1.15) of phen relative to K_2PtCl_4 was dissolved in a minimum amount of 0.01 M HCl. The solution was heated to 100°C, and then a solution of K_2PtCl_4 in water was added drop-wise to the reaction mixture. This mixture was then heated at reflux for 3 hours, after which time a yellow solid formed. This solid was filtered, washed with plenty of water, and then dried under vacuum. A 95% yield of crude yellow solid was obtained, which was judged to be the desired product on the basis of the observed color change.[12]

5.4 Synthesis of [Pt(phen)(EDMA)]Cl_2

[Pt(phen)(EDMA)]Cl_2 was then synthesized by dissolving 5 equivalents of the EDMA ligand in water. Once dissolved, [Pt(phen)Cl_2] was added to the reaction flask, and the reaction was heated at reflux, until a clear pale yellow solution formed. Upon cooling, the yellow solution was filtered to remove any unreacted [Pt(phen)Cl_2], and the volatiles were removed under reduced pressure. A pale yellow solid was left behind, which was considered on the basis of ^{1}H NMR spectroscopy to contain unreacted EDMA. The unwanted EDMA was removed by selective precipitation of the Pt complex. This was achieved by dissolving the crude material in a minimum volume of a 1:3 acetone/water solution (v/v). Once the dissolution was achieved, diethyl ether was layered on top of the

solution. The solution was kept in the dark overnight, and the pale yellow precipitate that formed was collected by filtration and washed with acetone and diethyl ether. On a 150 mg scale with respect to [Pt(phen)Cl_2], 85 mg of [Pt(phen)(EDMA)]Cl_2 was obtained (51% yield). The product was characterized by ESI-MS (positive mode), ^{1}H NMR, and UV-vis.

The low-resolution ESI-MS data proved consistent with the formation of the desired complex. [Pt(phen)(EDMA)]Cl_2 was detected as $[M]^{2+}$ at 246, $[M-H]^+$ at 492, $[M+Cl]^+$ at 528 m/z, where M = $C_{16}H_{18}N_4O_2Pt$. The UV-vis absorbance spectra of phen and [Pt(phen)(EDMA)]Cl_2 are given in Figure 5.4.1. A clear red-shift of the peak at 267 nm, ascribed to the phen subunit, to 276 nm in the complex is observed. Such a shift is in line

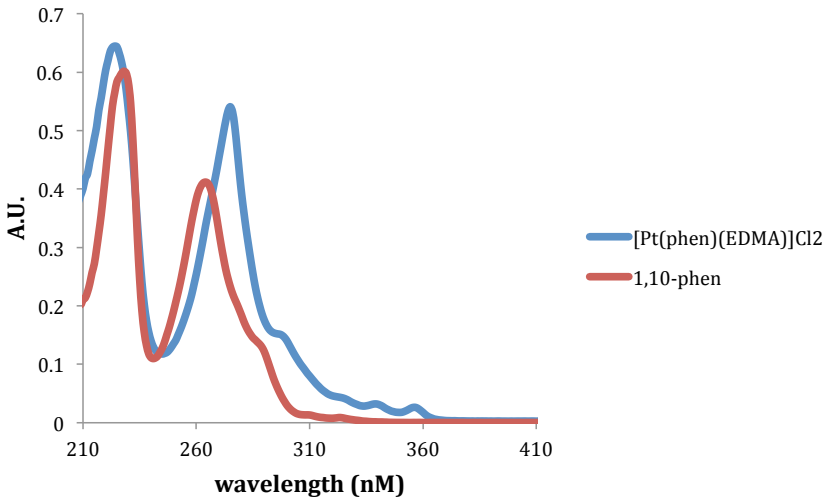

Figure 5.3 UV-vis absorbance spectrum of 1,10-phen in phosphate buffered saline, with HCl added to help dissolution. Also shown is the absorbance spectrum of [Pt(phen)(EDMA)]Cl_2. A Cary 5000 UV-vis-NIR spectrometer was used for these measurements.

with related literature examples for complexes of this type.[14] The ^{1}H NMR spectrum of [Pt(phen)(EDMA)]Cl_2 (400 MHz, D_2O) is shown in Figure 5.4.2. Peak integration was normalized to the sharp singlet at 7.96 ppm, which was assigned to the 2 protons at the 5 and 6 positions on the phen backbone. From the integration of the other peaks in both the

aliphatic and aromatic regions of the spectrum, all protons of the complex are accounted for, except the protons bound to the N atoms of the EDMA moiety, as these cannot be readily observed in a D_2O solvent system. Taken together, the analytical data provide support for the successful synthesis of [Pt(phen)(EDMA)]Cl_2. A SciFinder search failed to reveal any prior mention of this complex.

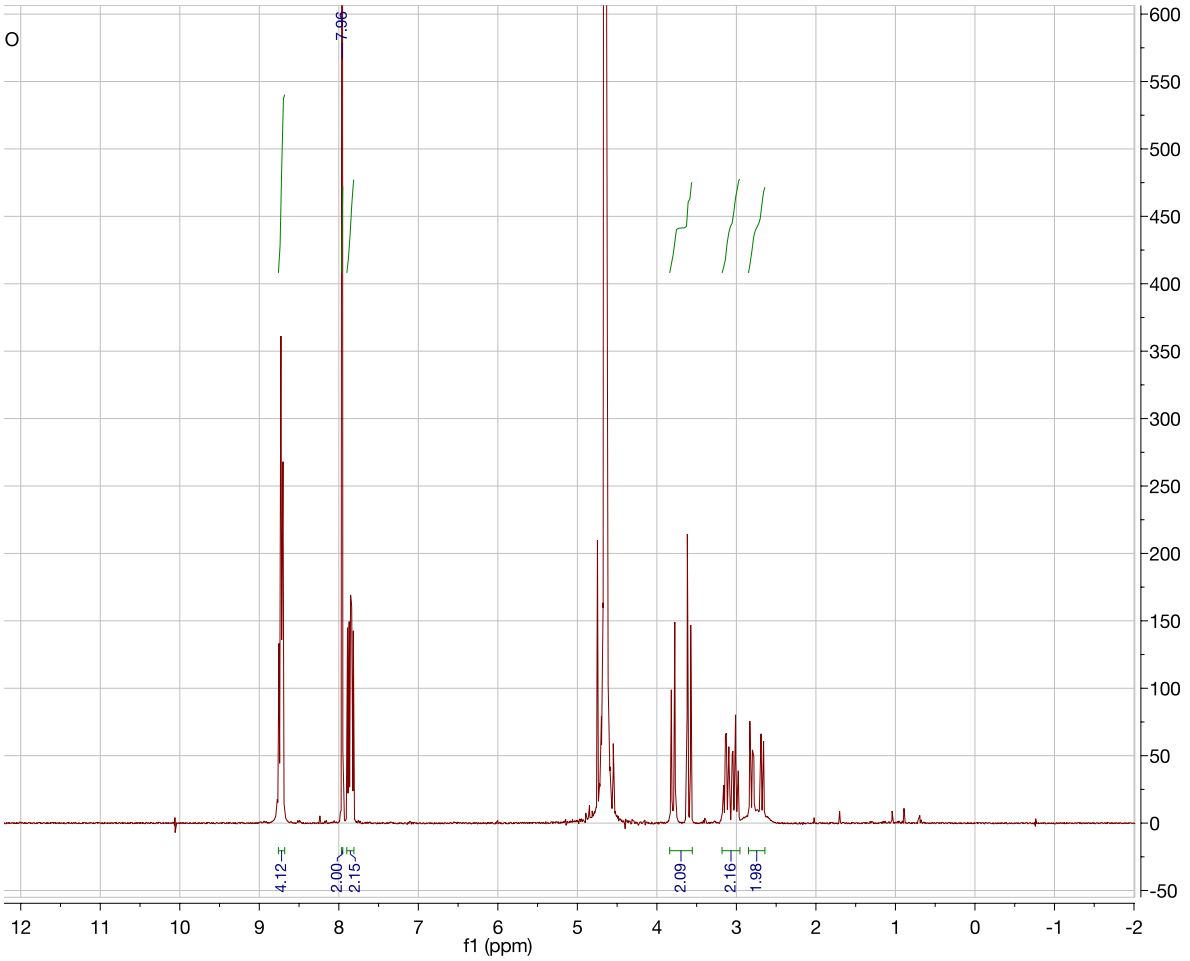

Figure 5.4 ^{1}H NMR (400 MHz, D_2O) spectrum of [Pt(phen)(EDMA)]Cl_2. δ = 8.72 (4H, m), 7.96 (2H, s), 7.84 (2H, m), 3.67 (2H, appt dd, J = 86.1, J = 17.3), 3.05 (2H, appt dtd, J = 45.4, J = 13.35, J = 4.01), 2.72 (2H, appt dd, J = 54.01, J = 4.01).

5.5 Synthetic attempts for the desired anticancer conjugate

The attempted synthetic conditions for the synthesis of MGd-PtInter1 are shown in Figure 5.5.1. Reactions were monitored using the same RP-HPLC conditions described in

previous chapters. ESI-MS (positive mode) was used to confirm or refute the presence of MGd-PtInter1 in the crude reaction mixtures. The first coupling agent tried was 1,1'-carbonyldiimidazole (CDI) because it had been previously reported to give good yields in the coupling of [Pt(EDMA)Cl_2] to primary amines.[15] The reaction was performed on a 3 mg scale in relation to the mono-amine derivative of MGd (CH_3COO^-), which was synthesized using MGd obtained as a gift to the Sessler Group from Pharmacyclics, Inc. A slight excess of CDI (1.15 equivalents) was dissolved in DMF, and this was added to a stirred solution of

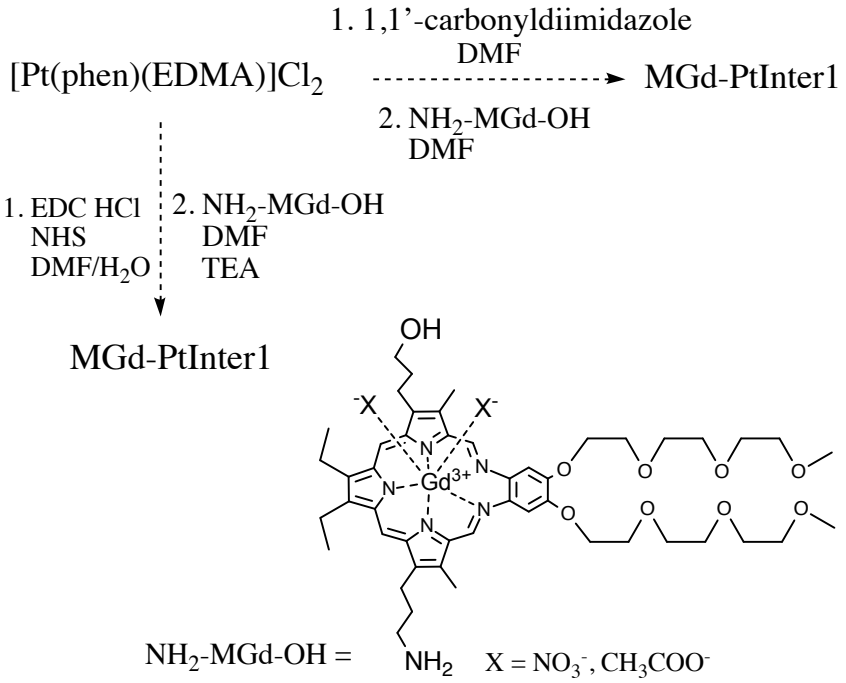

Figure 5.5. Attempted syntheses of MGd-PtInter1. EDC HCl = N-(3-dimethylaminopropyl)-N'-ethylcarbodiimide hydrochloride, NHS = N-hydroxy succinimide, TEA = triethylamine

[Pt(phen)(EDMA)]Cl_2 in DMF. The reaction flask was heated at 60°C for 10 minutes, after which time the mono-amine derivative of MGd was added to the flask drop-wise. The reaction was left stirring overnight, and the next day HPLC analysis was used to gauge the success of the reaction (Figure 5.5.2). ESI-MS analysis of the crude gave a peak that is

thought to be the desired product ($[M+2(HCOO^-)-(H^+)]^+$ at 1592 m/z (M = $C_{64}H_{83}N_{10}O_{10}GdPt$)). The product mass was assigned on the basis of the apparent Gd^{3+}/Pt^{2+} isotope pattern.

The peak at 2.3 min. in the HPLC chromatogram corresponds to $[Pt(phen)(EDMA)]Cl_2$, while the peak at 6.8 min. is the mono-amine MGd derivative. The mono-amine MGd was almost exclusively converted to a new species, as inferred from the observation of a peak at 7.2 min. The peak at 7.2 min. was isolated using a Sep-Pak tC18 column, using acetonitrile and 0.1% acetic acid in water as the eluent. When the isolated fraction at 7.2 min. was tested for the presence of MGd-PtInter1, no Pt^{2+} or Gd^{3+}/Pt^{2+} isotopes were observed. When the purified fraction was re-injected onto the RP-HPLC, the same retention time of 7.2 min. was observed. Therefore, the fraction was isolated intact.

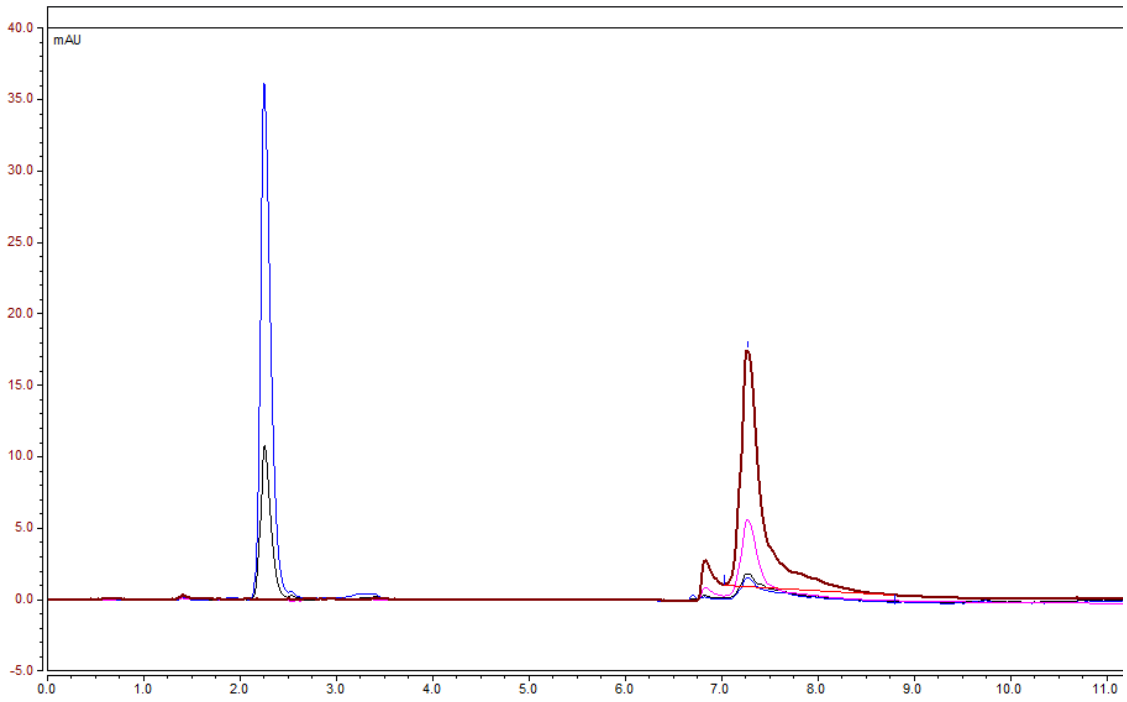

Figure 5.6 Partial RP-HPLC chromatogram of the reaction mixture of $[Pt(phen)(EDMA)]Cl_2$ and mono-amine MGd, after reacting in the presence of 1,1'-carbonyldiimidazole. Wavelengths monitored include 254 nm (black), 275 nm (blue), 740 nm (pink), and 470 nm (brown).

On this basis, it was concluded that the major product of the reaction was actually a side product that was the result of coupling between the primary amine of mono-amine MGd and acetate (By ESI-MS: $[M+HCOO^-]^+$ at 1116 m/z; M = $C_{50}H_{69}N_6O_{10}Gd$). The same observations were made upon analyzing the RP-HPLC and ESI-MS of the crude reaction mixture, when EDC HCI/NHS were used as the coupling agents. The source of the acetate was likely coming from the counter ion of MGd, and so it was concluded that the –COOH appendage of $[Pt(phen)(EDMA)]Cl_2$ is not very reactive under the conditions tested, or at least when a more reactive nucleophile (in this case acetate) is present. Therefore, the nitrate derivative of mono-amine MGd was used instead.

The conditions that appeared to work best for this coupling reaction involved the use of EDC HCl and NHS coupling agents. Briefly, 1.5 equivalents of NHS and 2.5 equivalents of EDC HCl (relative to the primary amine) were dissolved in DMF. 1.5 equivalents of the $[Pt(phen)(EDMA)]Cl_2$ complex (relative to the primary amine) was dissolved in a minimum amount of water. This was then added drop-wise to a stirred solution of the EDC HCl/NHS coupling agents. After 15 minutes, a solution of the mono-amine MGd (NO_3^-) in DMF, with an equimolar amount of triethylamine, was added drop-wise to the activated Pt complex. After a two-day reaction period, the reaction was deemed complete. From the RP-HPLC chromatogram shown in Figure 5.5.3, it was inferred that most of the mono-amine MGd starting material was converted to a new species characterized by a broad peak at 7.4 min in the HPLC chromatogram. The new peak at 7.4 min has greater absorbance at 275 nm than 254 nm. This was an indication that the desired coupling product might be formed, as the unreacted mono-amine MGd has a signature spectrum of decreasing absorbance across the series: 470, 740, 254, and 275 nm. Since the $[Pt(phen)(EDMA)]Cl_2$ has strong

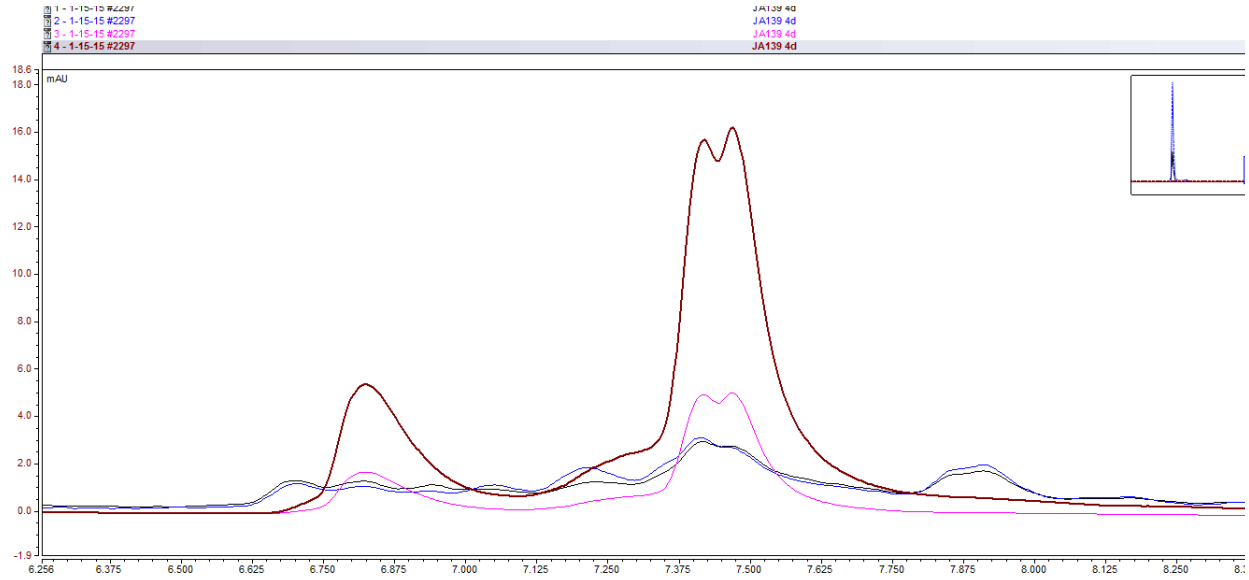

Figure 5.7 Partial RP-HPLC chromatogram for the crude reaction mixture between [Pt(phen)(EDMA)]Cl_2 and mono-amine MGd as observed after reaction with EDC HCI and NHS coupling agents. Wavelengths monitored include 470 nm (brown), 740 nm (pink), 275 nm (blue), and 254 nm (black).

absorbance at 275 nm, it can be inferred that the switch in the order of absorbance peak intensity for the species eluting at 7.4 min (to: 470, 740, 275, and 254 nm-decreasing in absorbance intensity across the series) was caused by the linking of a [Pt(phen)(EDMA)]Cl_2 subunit to the MGd core. Evidence for MGd-PtInter1 formation came from an ESI-MS analysis, where a peak at 1518 m/z was seen. This peak is attributed to $[M-(2H^+)+(OH^-)]^+$ ($M = C_{64}H_{83}N_{10}O_{10}GdPt$).

On the basis of the author's findings, one can conclude that the coupling reaction between mono-amine MGd and [Pt(phen)(EDMA)]Cl_2 is a very finicky reaction. It needs to be performed under very specific conditions to get an appreciable amount of product. Under all coupling reaction conditions tested, the peak at 2.3 min. corresponding to [Pt(phen)(EDMA)]Cl_2 remained intact and in high intensity. This is consistent with this complex not being readily activated under any of the conditions tested. This lack of

reactivity could be due to steric hindrance around the –COOH group of the Pt complex. It is also possible that the nucleophilicity of –COOH is decreased due to weak electrostatic interactions with the electropositive metal center.

5.6 Conclusion

In conclusion, a new complex, $[Pt(phen)(EDMA)]Cl_2$, was synthesized. It was characterized by a combination of ^1H NMR, UV-vis, and ESI-MS. This complex was designed to serve as a precursor for creating a new anticancer pro-drug, wherein a $[Pt(phen)(en)]Cl_2$ derivative is linked to MGd. Although preliminary analytical data were consistent with the desired conjugate, MGd-PtInter1, being formed under certain reaction conditions, it could not be isolated cleanly from the crude reaction mixture. Since the reactions were performed on a 1-5 mg scale, which was too small for efficient separation on a Sep-Pak tC18 column, it is possible that future work will allow this product to be obtained in clean form. Efforts are also underway to create second generation $[Pt(phen)(en)]Cl_2$ derivatives containing more reactive carboxylic acid functionalities.

5.7 References

[1] Lippard, S. J. *Acc. Chem. Res.*, **1978**, 11, 211-217.
[2] Sammes, P. G. Yahioglu, G. *Chem. Soc. Rev.*, **1994**, 23, 327-334.
[3] Otto, D. Ihmels, H. *Top Curr Chem*., **2005**, 258, 161-204.
[4] Pages, B. J. Ang, D. L. Wright, E. P. Aldrich-Wright, J. R. *Dalton Trans*., **2015**, 44, 3505-3526.
[5] Wheate, N. J. Taleb, R. I. Krause-Heuer, A. M. Cook, R. L. Wang, S. Higgins, V. J. Aldrich-Wright, J. R. *Dalton Trans.*, **2007**, 43, 5055-5064.
[6] Krause-Heuer, A. M. Wheate, N. J. Tilby, M. J. Pearson, G. Ottley, C. J. Aldrich-Wright, J. R. *Inorg. Chem.*, **2008**, 47, 6880-6888.
[7] Preihs, C. Arambula, J. F. Magda, D. Jeong, H. Yoo, D. Cheon, J. Siddik, Z. H. Sessler, J. L. *Inorg. Chem.*, **2013**, 52, 12184-12192.

[8] Thiabaud, G. Arambula, J. F. Siddik, Z. H. Sessler, J. L. *Chem. Eur. J.*, **2014**, 20, 8942-8947.
[9] Sessler, J. L. Arambula, J. Siddik, Z. H. Thiabaud, G. Texaphyrin-pt(iv) conjugates and compositions for use in overcoming platinum resistance. US20170246182A1, Jun 11, 2014.
[10] Reedjik, J. *Chem. Rev.*, **1999**, 99, 2499-2510.
[11] Patureau, B. M. Hudson, R. H. E. Damha, M. J. *Bioconjugate Chem.*, **2007**, 18, 421-430.
[12] Beibei, L. Huo, S. Ren, Y. Sun, S. Cao, Z. Shen, S. *Transition Met Chem*., **2015**, 40, 31-37.
[13] Zhao, X. Zhang, Y. Hou, X. Shi, J. Shen, S. Huo, S. *Transit Met Chem*., **2017**, 42, 219-228.
[14] Pages, B. J. Li, F. Wormell, P. Ang, D. L. Clegg, J. K. Kepert, C. J. Spare, L. K. Danchaiwijit, S. Aldrich-Wright, J. R. *Dalton Trans.*, **2014**, 43, 15566-15575.
[15] Wilson, J. J. Lippard, S. J. *Inorganica Chimica Acta*, **2012**, 389, 77-84.

Chapter 6: Supplementary Data

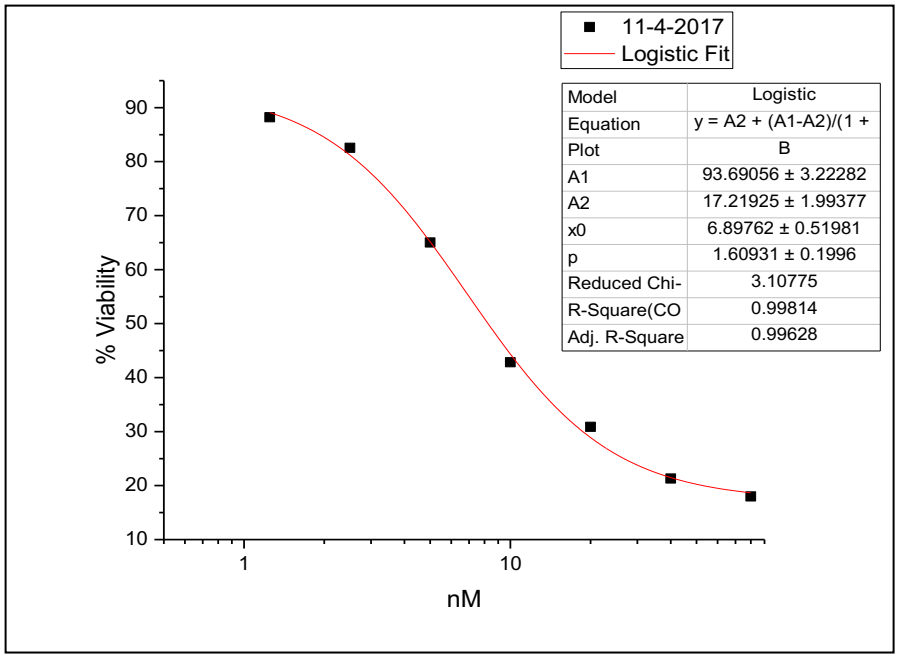

Figure 6.1 Logistic Fit of cell viability data for A549 cells incubated with Dp44mT (80-1.25 nM) over a 3-day period. Data was normalized to the control (cells incubated without Dp44mT).

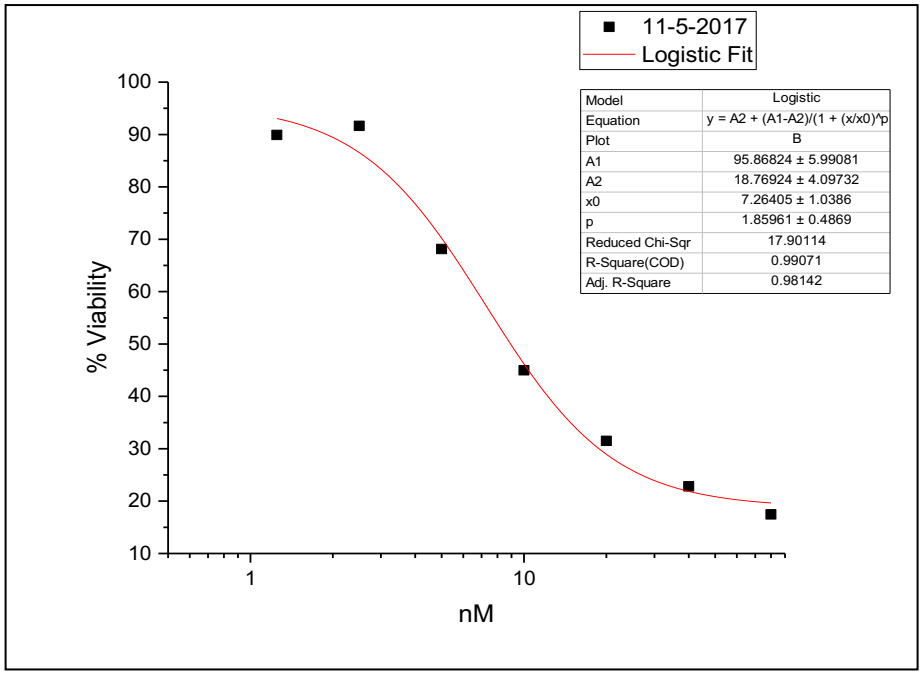

Figure 6.2 Logistic Fit of cell viability data for A549 cells incubated with Dp44mT (80-1.25 nM) over a 3-day period. Data was normalized to the control (cells incubated without Dp44mT).

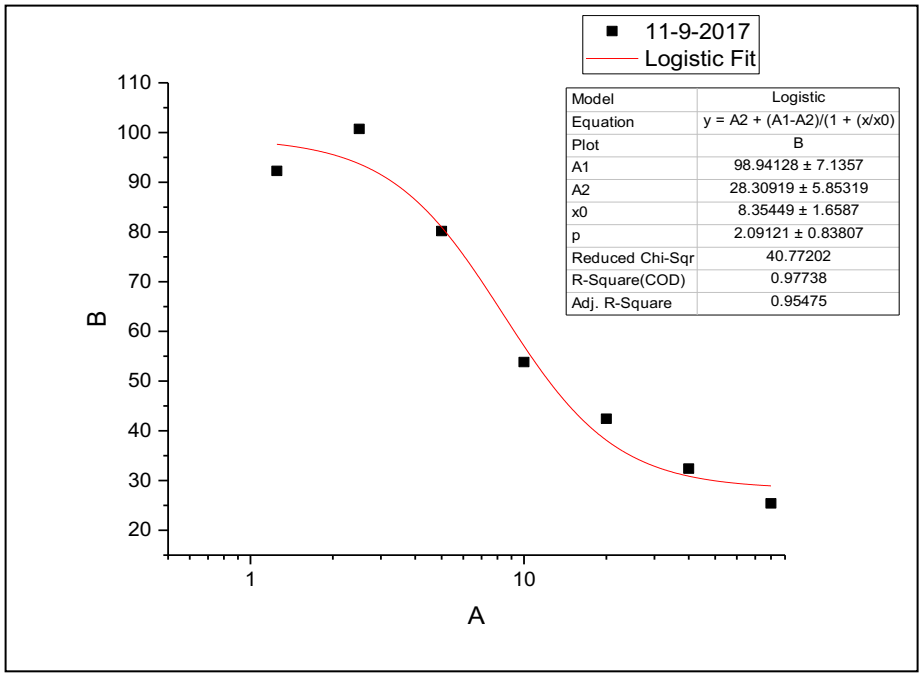

Figure 6.3 Logistic Fit of cell viability data for A549 cells incubated with Dp44mT (80-1.25 nM) over a 3-day period. Data was normalized to the control (cells incubated without Dp44mT). A = nM concentration of Dp44mT B = % viability

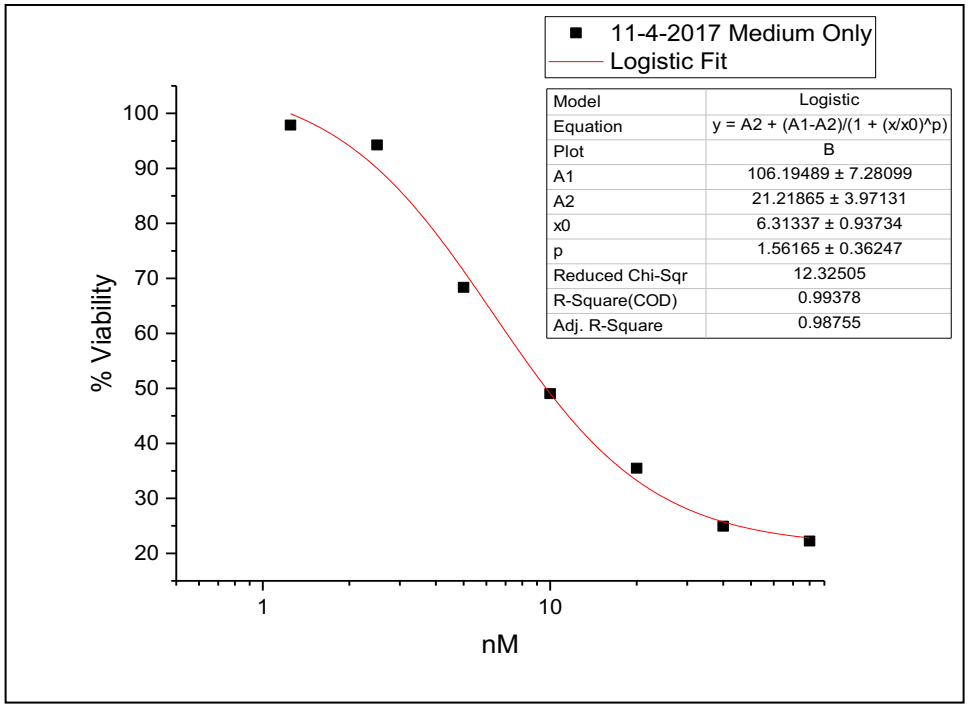

Figure 6.4 Logistic Fit of cell viability data for A549 cells incubated with Dp44mT+100 µM MGd over a 3-day period. Data was normalized to the control (cells incubated without Dp44mT/MGd). Concentration range of Dp44mT: 80-1.25 nM.

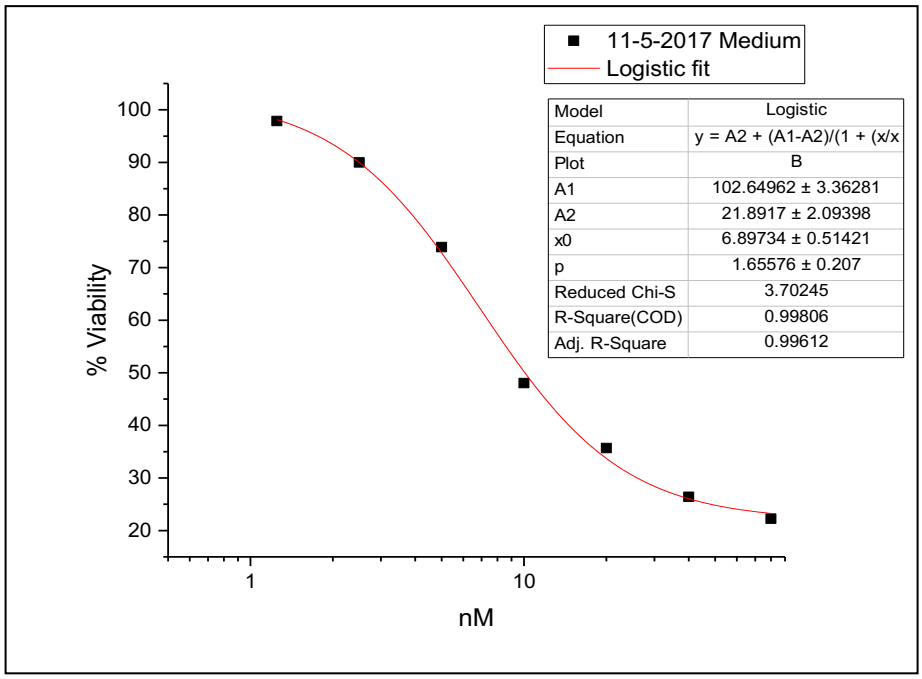

Figure 6.5 Logistic Fit of cell viability data for A549 cells incubated with Dp44mT+100 µM MGd over a 3-day period. Data was normalized to the control (cells incubated without Dp44mT/MGd). Concentration range of Dp44mT: 80-1.25 nM.

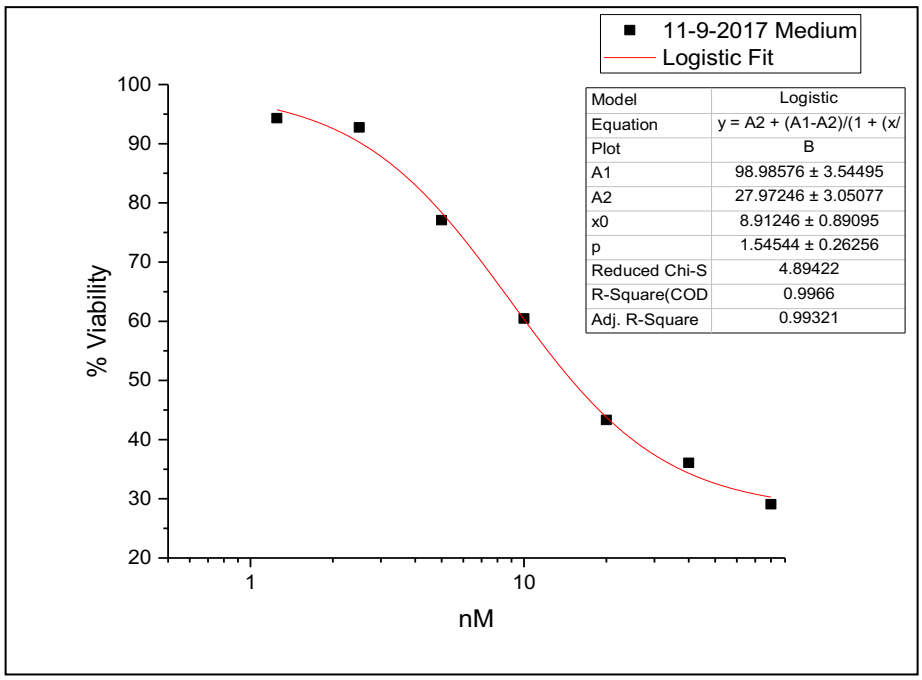

Figure 6.6 Logistic Fit of cell viability data for A549 cells incubated with Dp44mT+100 µM MGd over a 3-day period. Data was normalized to the control (cells incubated without Dp44mT/MGd). Concentration range of Dp44mT: 80-1.25 nM.

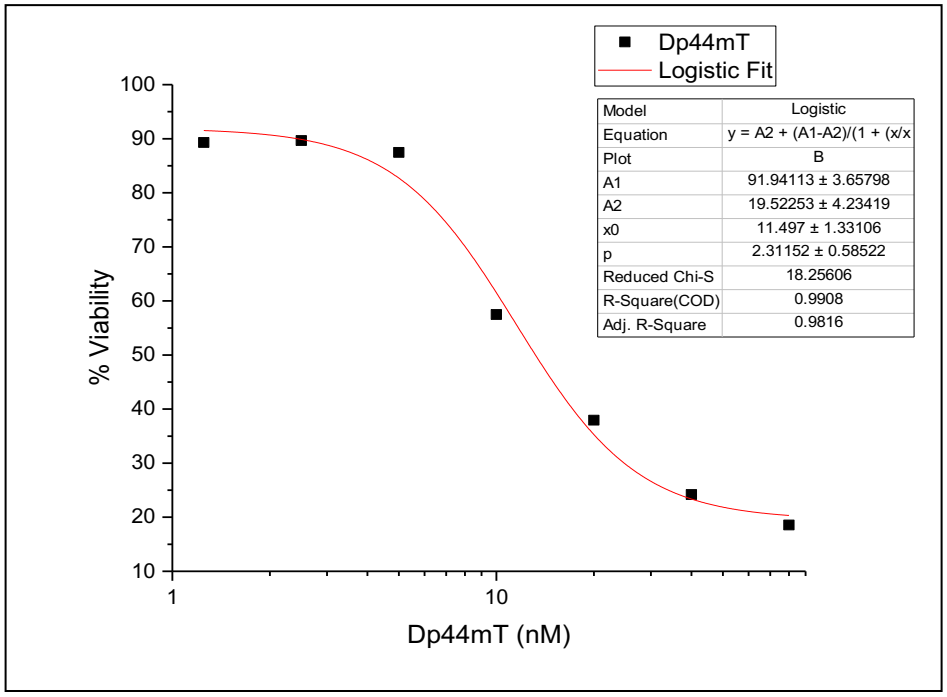

Figure 6.7 Logistic Fit of cell viability data for A549 cells incubated with Dp44mT (80-1.25 nM) over a 3-day period. Data was normalized to the control (cells incubated without Dp44mT).

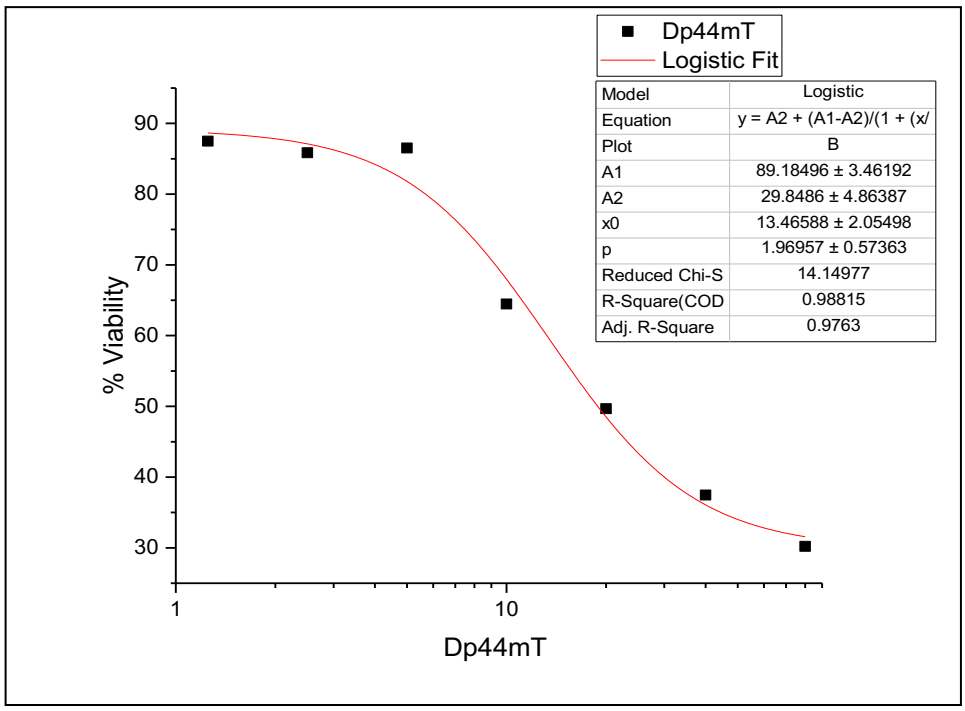

Figure 6.8 Logistic Fit of cell viability data for A549 cells incubated with Dp44mT (80-1.25 nM) over a 3-day period. Data was normalized to the control (cells incubated without Dp44mT).

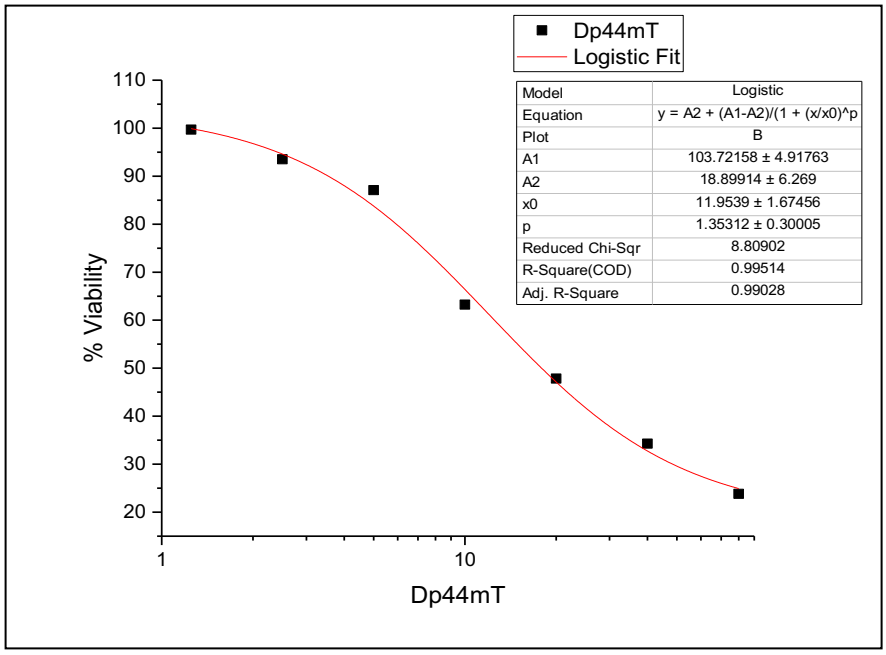

Figure 6.9 Logistic Fit of cell viability data for A549 cells incubated with Dp44mT (80-1.25 nM) over a 3-day period. Data was normalized to the control (cells incubated without Dp44mT).

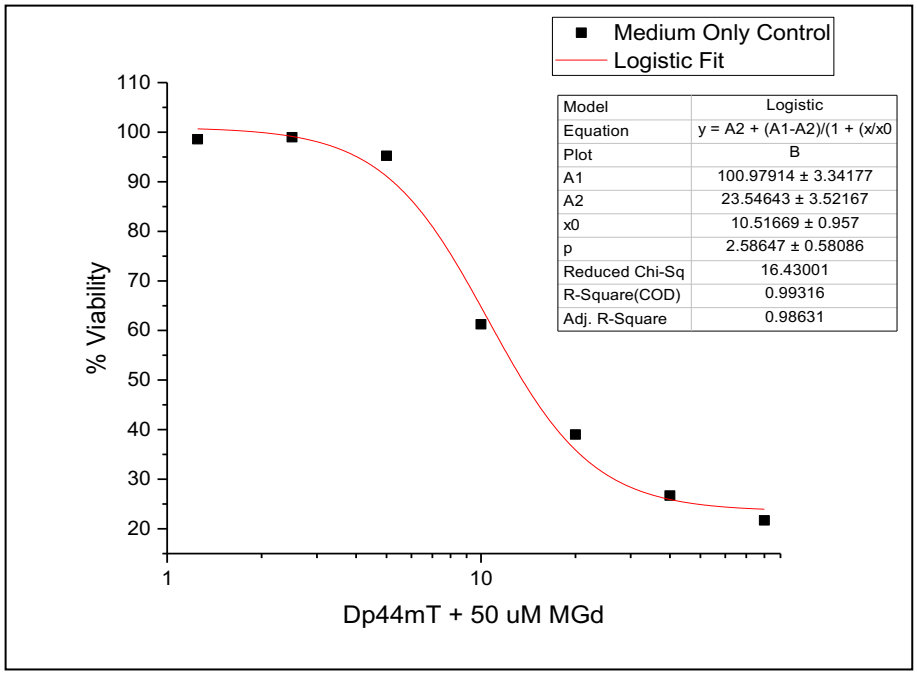

Figure 6.10 Logistic Fit of cell viability data for A549 cells incubated with Dp44mT+50 µM MGd over a 3-day period. Data was normalized to the control (cells incubated without Dp44mT/MGd). Concentration range of Dp44mT: 80-1.25 nM.

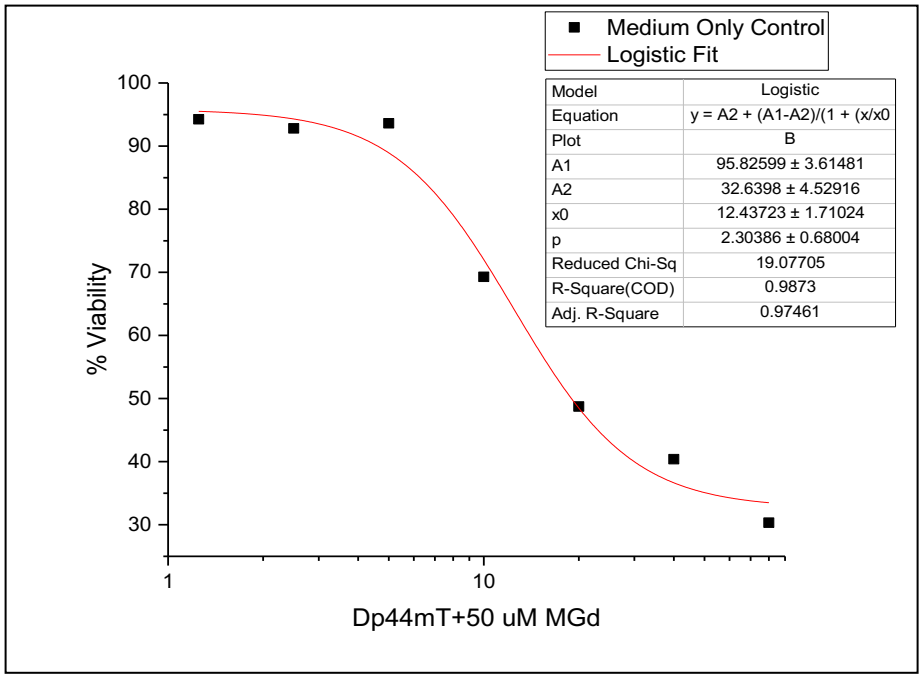

Figure 6.11 Logistic Fit of cell viability data for A549 cells incubated with Dp44mT+50 µM MGd over a 3-day period. Data was normalized to the control (cells incubated without Dp44mT/MGd). Concentration range of Dp44mT: 80-1.25 nM.

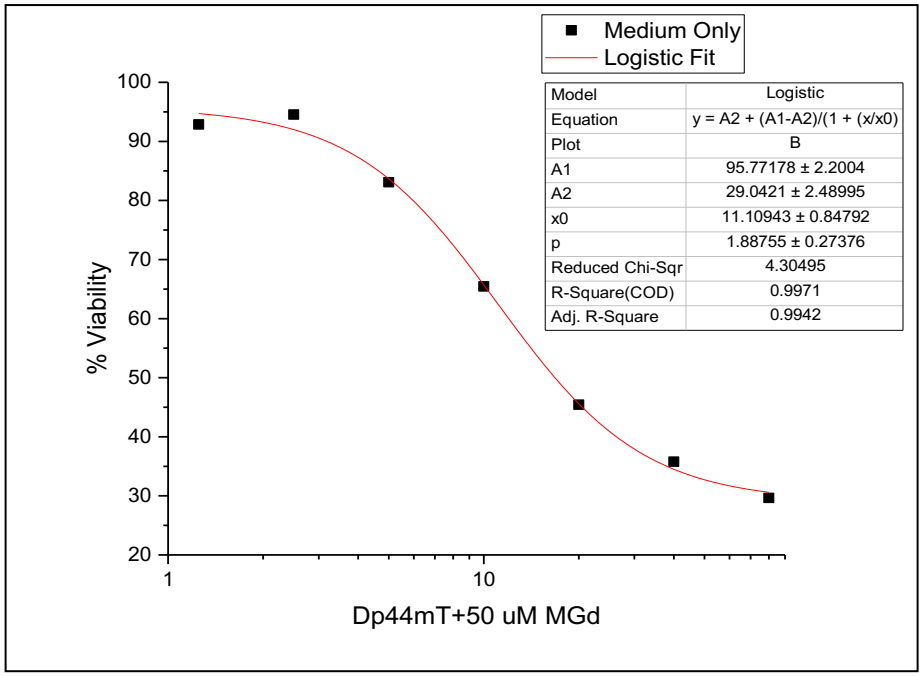

Figure 6.12 Logistic Fit of cell viability data for A549 cells incubated with Dp44mT+50 µM MGd over a 3-day period. Data was normalized to the control (cells incubated without Dp44mT/MGd). Concentration range of Dp44mT: 80-1.25 nM.

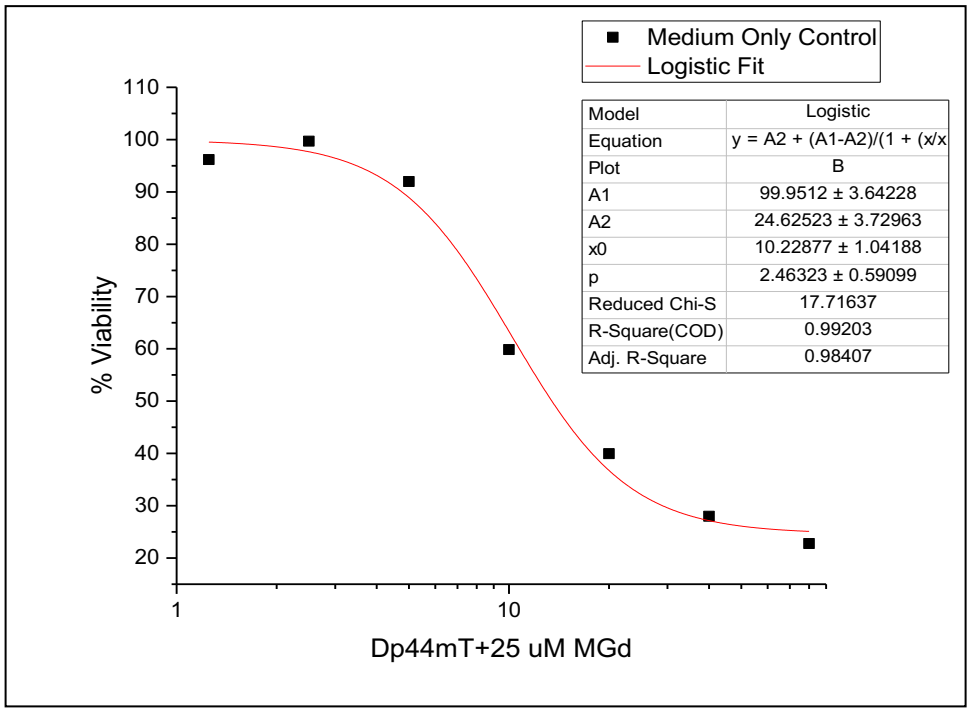

Figure 6.13 Logistic Fit of cell viability data for A549 cells incubated with Dp44mT+25 µM MGd over a 3-day period. Data was normalized to the control (cells incubated without Dp44mT/MGd). Concentration range of Dp44mT: 80-1.25 nM.

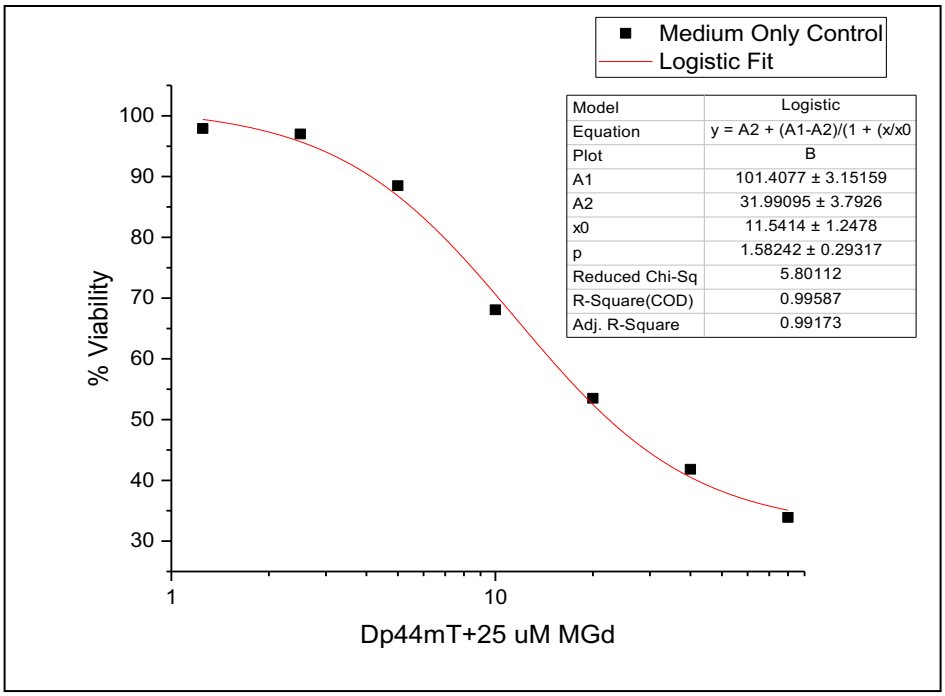

Figure 6.14 Logistic Fit of cell viability data for A549 cells incubated with Dp44mT+25 µM MGd over a 3-day period. Data was normalized to the control (cells incubated without Dp44mT/MGd). Concentration range of Dp44mT: 80-1.25 nM.

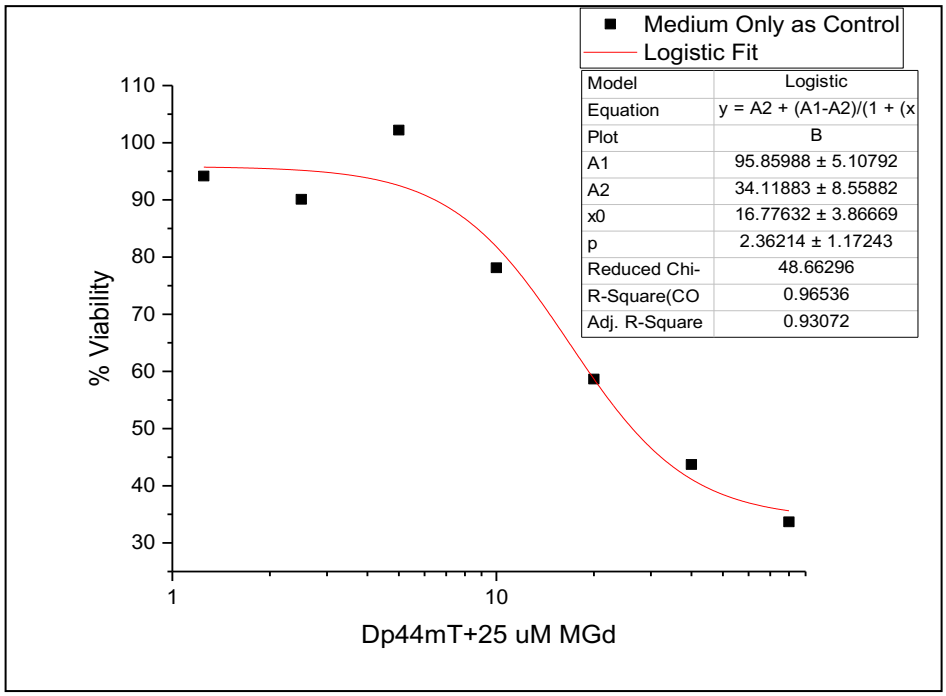

Figure 6.15 Logistic Fit of cell viability data for A549 cells incubated with Dp44mT+25 µM MGd over a 3-day period. Data was normalized to the control (cells incubated without Dp44mT/MGd). Concentration range of Dp44mT: 80-1.25 nM.

References

[1] Sessler, J. L. Murai, T. Lynch, V. Cyr, M. *J. Am. Chem. Soc.*, **1988**, 110, 5586-5588.

[2] Hannah S. Lynch, V. M. Gerasimchuk, N. Magda, D. Sessler, J. L. *Org. Lett.*, **2001**, 3, 3911-3914.

[3] Zhou, Z. and Lu, Z. *Wiley Interdiscip Rev Nanomed Nanobiotechnol*., **2013**, 5, 1-18.

[4] Idee, J. Port, M. Raynal, I. Schaefer, M. Greneur, S. Corot, C. *Fundamental and Clinical Pharmacology*, **2006**, 20, 563-576.

[5] Arambula, J. F. Preihs, C. Borthwick, D. Magda, D. Sessler, J. L. *Anticancer Agents Med Chem.*, **2011**, 11, 222-232.

[6] Preihs, C. Arambula, J. F. Magda, D. Jeong, H. Yoo, D. Cheon, J. Siddik, Z. H. Sessler, J. L. *Inorg. Chem.*, **2013**, 52, 12184-12192.

[7] Sessler, J. L. Tvermoes, N. A. Guldi, D. M. Mody T. D. Allen, W. E. *J. Phys. Chem. A.*, **1999**, 103, 787-794.

[8] Magda, D. Gerasimchuk, N. Lecane, P. Miller, R. A. Biaglow, J. E. Sessler, J. L. *Chem. Commun.*, **2002**, 2730-2731.

[9] Sessler, J. L. Tvermoes, N. A. Guldi, D. M. Hug, G. L. Mody, T. D. Magda, D. *J. Phys. Chem. B*, **2001**, 105, 1452-1457.

[10] Meyers, C. A. Smith, J. A. Bezjak, A. Mehta, M. P. Liebmann, J. Illidge, T. Kunkler, I. Caudrelier, J. Eisenberg, P. D. Meerwaldt, J. Siemers, C. C. Gaspar, L. E. Curran, W. Phan, S. Miller, R. A. Renschler, M. F. *Journal of Clinical Oncology*, **2004**, 22, 157-165.

[11] Lee, M. H. Kim, E. Lee, H. Park, S. Y. Hong, K. S. Kim, J. S. Sessler, J. L. *Chem. Commun.*, **2016**, 52, 10551-10554.

[12] Wei, W. Fountain, M. E. Sessler, J. L. Magda, D. J. Wang, Z. Miller, R. A. *Macrocyclic Chemistry: Current Trends and Future Perspectives*, 407-425.

[13] Thiabaud, G. Arambula, J. F. Siddik, Z. H. Sessler, J. L. *Chem. Eur. J.*, **2014**, 20, 8942-8947.

[14] Sessler, J. L. Arambula, J. Siddik, Z. H. Thiabaud, G. Texaphyrin-pt(iv) conjugates and compositions for use in overcoming platinum resistance. US20170246182A1, Jun 11, 2014.

[15] Lovejoy, D. B. Sharp, D. M. Seebacher, N. Obeidy, P. Prichard, T. Stefani, C. Basha, M. T. Sharpe, P. C. Jansson, P. J. Kalinowski, D. S. Bernhardt, P. V. Richardson, D. R. *Journal of*

Medicinal Chemistry, **2012**, 55, 7230-7244.

[16] Lippard, S. J. *Acc. Chem. Res.*, **1978**, 11, 211-217.

[17] Aime, S. Botta, M. Fasano, M. Terreno, E. *Chemical Society Reviews*, **1998**, 27, 19-29.

[18] Caravan, P. Ellison, J. J. McMurry, T. J. Lauffer, R. B. *Chem. Rev.*, **1999**, 99, 2293-2352.

[19] Caravan, P. *Chem. Soc. Rev.*, **2006**, 35, 512-523.

[20] Qiu, L. Zhang, F. Shi, Y. Bai, Z. Wang, J. Li, Y. Lee, D. Ingraham, C. Feng, X. Yang, X. *Radiology*, **2016**, 279, 400-409.

[21] Ford, J. M. Seiferheld, W. Alger, J. R. Wu, G. Endicott, T. J. Mehta, M. Curran, W. Phan, S. *International Journal of Radiation Oncology Biology Physics*, **2007**, 69 831-838.

[22] Manon, R. Hui, S. Chinnaiyan, P. Suh, J. Chang, E. Timmerman, R. Phan, S. Das, R. Mehta, M. *Technology in Cancer Research & Treatment*, **2004**, 3, 303-307.

[23] Hirschberg, H. Wu, G. N. Madsen, S. J. *Minim. Invasive Neurosurg.*, **2007**, 50, 318-323.

[24] Li, W. Zhou, G. Mak, T. C. W. *Advanced Structural Inorganic Chemistry*, Oxford University Press: New York, 2008; p 54-63 and 685-687.

[25] Rinehart, J. D. and Long, J. R. *Chem. Sci.*, **2011**, 2 2078-2085.

[26] Zhang, P. Gui, Y. Tang, J. *Coordination Chemistry Reviews*, **2013**, 257, 1728-1763.

[27] Sessoli, R. Tsai, H. L. Schake, A. R. Wang, S. Vincent, J. B. Folting, K. Gatteschi, D. Christou G. and Hendrickson, D. N. *J. Am. Chem. Soc.*, **1993**, 115, 1804–1816.

[28] Ishikawa, N. Sugita, M. Ishikawa, T. Koshihara, S. Kaizu, Y. *J. Am. Chem. Soc.*, **2003**, 125, 8694-8695.

[29] Chen, Y, Liu, J. Ungur, L. Liu, J. Li, Q. Wang, L. Ni, Z. Chibotaru, L. F. Chen, X. Tong, M. *J. Am. Chem. Soc.*, **2016**, 138, 2829-2837.

[30] Li, J. Yuan, C. Yang, L. Kong, M. Zhang, J. Ge, J. Zhang, Y. Song, Y. *Inorganic Chemistry*, **2017**, 56, 7835-7841.

[31] Gavey, E. L. Beldjoudi, Y. Rawson, J. M. Stamatatos, T. C. Pilkington, M. *Chem. Commun.*, **2014**, 50, 3741-3743.

[32] Guldi, D. M. Mody, T. D. Gerasimchuk, N. N. Magda, D. Sessler, J. L. *J. Am. Chem. Soc.*, **2000**, 122, 8289-8298.

[33] Lisowski, J. Sessler, J. L. Lynch, V. Mody, T. D. *J. Am. Chem. Soc.*, **1995**, 117, 2273-2285.

[34] Preihs, C.; Magda, D. J.; Sessler, J. L. *Bioinorg React Mech.*, **2013**, 9, 3-14.

[35] Arambula, J. F.; Sessler, J. L.; Siddik, Z. H. *Medchemcomm*., **2012**, 3, 1275-1281.

[36] Yu, Y. Kalinowski, S. Kovacevic, Z. Siafakas, A. R. Jansson, P. J. Stefani, C. Lovejoy, D. B. Sharpe, P. C. Bernhardt, P. V. Richardson, D. R. *J. Med. Chem.*, **2009**, 52, 5271-5294.
[37] Seebacher, N. A.; Richardson, D. R.; Jansson, P. J. *Cell Death and Disease*, **2016**, 7, 1-13.
[38] Woodburn, K. W. *The Journal of Pharmacology and Experimental Therapeutics*, **2001**, 297, 888-894.
[39] Kim, J. Kim, J. Bae, J. *Experimental and Molecular Medicine*, **2016**, 28, 1-13.
[40] Thiabaud, G. McCall, R. He, G. Arambula, J. F. Siddik, Z. H. Sessler, J. L. *Angew. Chem. Int. Ed.*, **2016**, 55, 12626, 12631.
[41] Sammes, P. G. Yahioglu, G. *Chem. Soc. Rev.*, **1994**, 23, 327-334.
[42] Otto, D. Ihmels, H. *Top Curr Chem*., **2005**, 258, 161-204.
[43] Pages, B. J. Ang, D. L. Wright, E. P. Aldrich-Wright, J. R. *Dalton Trans*., **2015**, 44, 3505-3526.
[44] Wheate, N. J. Taleb, R. I. Krause-Heuer, A. M. Cook, R. L. Wang, S. Higgins, V. J. Aldrich-Wright, J. R. *Dalton Trans.*, **200**7, 43, 5055-5064.
[45] Krause-Heuer, A. M. Wheate, N. J. Tilby, M. J. Pearson, G. Ottley, C. J. Aldrich-Wright, J. R. *Inorg. Chem.*, **2008**, 47, 6880-6888.
[46] Reedjik, J. *Chem. Rev.*, **1999**, 99, 2499-2510.
[47] Patureau, B. M. Hudson, R. H. E. Damha, M. J. *Bioconjugate Chem.*, **2007**, 18, 421-430.
[48] Beibei, L. Huo, S. Ren, Y. Sun, S. Cao, Z. Shen, S. *Transition Met Chem*., **2015**, 40, 31-37.
[49] Zhao, X. Zhang, Y. Hou, X. Shi, J. Shen, S. Huo, S. *Transit Met Chem*., **2017**, 42, 219-228.
[50] Pages, B. J. Li, F. Wormell, P. Ang, D. L. Clegg, J. K. Kepert, C. J. Spare, L. K. Danchaiwijit, S. Aldrich-Wright, J. R. *Dalton Trans.*, **2014**, 43, 15566-15575.
[51] Wilson, J. J. Lippard, S. J. *Inorganica Chimica Acta*, **2012**, 389, 77-84.